AMORPHOUS SILICON SOLAR CELLS

B.W. CLARE, J.C.L. CORNISH, G.T. HEFTER, P.J. JENNINGS, C.P. LUND, G.O.M. TALUKDER AND G.P. THAMBIRASA

School of Mathematical and Physical Sciences
Murdoch University, Murdoch, WA 6150 Australia

J. LIVINGSTONE

Department of Electrical Engineering
University of Western Australia, WA 6009, Australia

C. KLAUBER

CSIRO Division of Minerals and Geochemistry
Bentley, WA 6102, Australia

Research Report : September 1988

ABSTRACT

Thin films of hydrogenated amorphous silicon have been prepared by chemical vapour deposition at atmospheric pressure from a mixture of silanes over a heated substrate. This approach provides an alternative method to glow discharge and it has several substantial advantages, including safety and lower costs.

Solar cells fabricated from these films show open circuit voltages of up to 400 mV but current densities are low. This has been attributed to a low hydrogen content in the films.

A wide range of analytical techniques has been established and used to characterise the material and confirm the low hydrogen content as a one of the obstacles to the production solar cell quality films

Modifications to the deposition technique are now proposed.

AMORPHOUS SILICON SOLAR CELLS

1. INTRODUCTION

This report describes the work carried out by the authors in 1987 on the continuation of the project described in our previous research report (Clare *et al* 1987) and includes the final part of the work funded under a grant from SERIWA and the final year's work under a grant from the CSIRO/Murdoch Collaborative Research Fund.

In the course of the year a number of aspects of the deposition and properties of hydrogenated amorphous silicon films have been investigated. We have continued to produce a-Si films by the thermal decomposition of a mixture of silanes at atmospheric pressure (APCVD). We have used a variety of substrates and have analysed the resultant films in a number of ways:

Auger electron Spectroscopy (AES) and X-ray photoelectron spectroscopy XPS) (section 3)

density of states using the space charge limited current (SCLC) technique (section 5)

infra-red spectroscopy (section 7)

optical spectroscopy (section 8)

electron microscopy (sections 9 and 10)

We have also made a preliminary investigation into alternative processes for the preparation of silanes (section 2), completed a detailed investigation into the most suitable grade of stainless steel for use as a substrate and developed an optimised preparation procedure (section 4). We have also gained greater understanding of some aspects of the CVD process by monitoring the gas flow with a quadrupole mass spectrometer (section 6).

Section 4 is essentially the text of a paper presented at the Solar World Congress in Hamburg October, 1987, and published in the proceedings of the congress by Pergamon Press.

Section 3 has been rewritten as a paper and submitted to Solar Energy Materials.

2. SYNTHESIS OF HIGHER SILANES

The three standard methods of preparing higher silanes are:

a. Reaction of magnesium silicide with acid.

b. Subjecting monosilane to a silent electric discharge.

c. Reacting higher chlorosilanes with lithium aluminium hydride.

Of these, only (b) gives a product of high purity. The method is described in several sources, e.g. Akhtar (1986). Silane thus produced contained no impurities down to 0.1 ppm. Silane from the magnesium silicide route contained appreciable amounts of hydrocarbons, and much carbon dioxide. Silanes from the chlorosilane route also contained hydrocarbons, and also chlorosilanes and chlorosiloxanes. Higher chlorosilanes are available as byproducts from the large scale manufacture of silicon tetrachloride. Preparation of pure silanes requires the use of pure magnesium silicide, formed by reaction of pure elements, rather than the thermite process which we have employed.

Experimental details for the reduction of silicon tetrachloride with lithium chloride are given in Inorganic Syntheses Vol. XI page 170 (A.D. Norman *et al*), a general procedure being given , but not specific details for the higher silanes. The preparation of higher chlorosilanes is given in Inorganic Syntheses, vol. 1, page 42. A mixture containing principally tetrachlorosilane, with 30% hexachlorodisilane, 4% octachlorotrisilane, and small amounts of higher chlorosilanes is prepared by passing chlorine over heated calcium silicon alloy. The reaction is complete in ca 2 weeks, and about 700 mls is obtained from 250 g of alloy.

3. AUGER LINESHAPE ANALYSIS AND THE STRUCTURE OF AMORPHOUS SILICON THIN FILMS PREPARED BY CVD

CVD is a promising technique for the production of thin films of a-Si:H, with deposition rates a factor of ten or more faster than glow discharge deposition. However Schottkjy barrier photo diodes fabricated from such films have poor performance compared to GD films. The techniques of Auger lineshape analysis, space charge limited current (SCLC) , thermal desorption (TDS) and infra-red spectroscopy (IRS) have been used to characterise the films and identify the reasons for their poor performance.

It has been shown that the LVV Auger lineshape for amorphous silicon is sensitive to the incorporation of hydrogen (Burnham and co-workers 1987, Madden 1983, Nelson and co-workers 1986, Zajac and Bader 1982). The change of lineshape with varying amounts of hydrogen has been reported for a-Si:H specimens prepared by glow discharge (GD) decomposition of silane and for crystalline specimens rendered amorphous by ion bombardment and hydrogenated with ion implanted hydrogen (Burnham and co-workers 1987, Madden 1983, Madden and Hjalmarson 1982, Nelson and co-workers 1986). The change in lineshape is explained in terms of three components: pp, sp, and localised two hole interaction L2H as described by Nelson and co-workers (1986) and Burnham and co workers (1987).

The SCLC technique is described in Section 5 and allows calculation of the band gap density of states (DOS). These states result from the dangling bonds that remain due to insufficient hydrogen incorporation in the silicon film. Hence the DOS values obtained relate to the hydrogen content in the films.

TDS is a direct method of determining the hydrogen content of the films and while it is destructive and rather cumbersome it does offer the possibility of a quantitative result (Cai and co-workers 1985, Fritzsche and co-workers 1979, McMillan and Peterson 1979, Morimoto and co-workers 1986). However, TDS does not appear to provide information about the bulk of the material, only the portion near the surface. It does not give direct information about the form of incorporation or the specific sites. This information is provided by IRS. (Shanks *et al* 1980, Yahya and Shanks 1987).

In this present work, we are primarily concerned with the degree of hydrogen incorporation in a-Si:h films prepared by atmospheric pressure chemical vapour deposition (APCVD) from a mixture of silanes generated in situ from the reaction of magnesium silicide with an acid (Kurtz, Proscia and Gordon 1986, Clare and co-workers 1987). These results are compared with the results for GD and ion implanted crystalline samples. It is well known that the temperatures required for a-Si:H film preparation by CVD are very much higher than the optimum for good hydrogen incorporation (Hegedus and co-workers 1986). Hence this study is part of an investigation of modifications and improvements to the CVD technique to produce films with better photovoltaic properties which are in turn influenced by the degree of hydrogenation.

3.1 Experimental Details

AES has been carried out in a Vacuum Generators' surface physics system equipped with an e'beam heating facility in addition to the usual analysis techniques. The samples of a-Si:H were cleaned by an optimised argon ion bombardment procedure (Lund 1987) which removes all detectable contaminants, principally oxygen, with minimum incorporation of A into the surface from the ion beam using low energy and flux of ions to minimise surface damage. Even so, the cleaning process was found to deplete the surface of hydrogen in the cases of hydrogenated CVD and GD samples. The surface hydrogen could however be restored by heating as a result of diffusion from the bulk of the film. Auger lineshape profiles were obtained using X-ray primary beam and in the N(E) mode for data collection. Background subtraction and scaling were carried out to facilitate comparisons of the spectra obtained. Decomposition of the profiles into their three components is not currently possible on our equipment, but the changes in these can be inferred from the marked changes in the lineshape that takes place allowing qualitative analysis at the stage.

TDS was carried out in a high vacuum system equipped with a resistively heated stage and a quadrupole mass spectrometer. A linear temperature ramp was provided by a computer.

IRS measurements were made on a Mattson Sirius 100 FTIR on samples prepared specifically for this purpose on crystalline silicon substrates. In order to get sufficient sensitivity these were the sum of three separate depositions, the substrates being held under flowing hydrogen between depositions. A fourth identical substrate was used as a reference in the FTIR.

SCLC measurements were made on films deposited on stainless steel substrates with evaporated aluminium top contacts.

With the exception of one sequence of films deposited at 650 C with the express intention of excluding hydrogen, all films were deposited under similar conditions at the minimum temperature for good deposition rate, 520C, and with He as the carrier gas for the silanes. Following deposition all samples were cooled to room temperature in flowing hydrogen except the 650C samples were cooled in flowing helium.

3.2 Results.

The Auger LVV lineshapes for samples of a-Si:H representing four different preparation and hydrogenation techniques are shown in figures 3.1 and 3.2.

The first sample (a) prepared from crystalline silicon before hydrogenation shows a pronounced low energy shoulder corresponding to the sp component, and a distinguishable high energy shoulder corresponding to the L2H component (figure 3.1). Hydrogenation by hydrogen ion implantation results in a slight reduction in the height of the pp component. Figure 3.2 shows that the peak of the pp component shifts to lower energies and there is a significant increase in the height of both the shoulders compared to the principal component, which on

deconvolution would be expected to show an increase in the areas corresponding to both the sp and L2H transitions with respect to the pp transition.

Samples (b) and (c) prepared by CVD and sample (d) prepared by GD show similar features immediately after cleaning and after heating samples (b) and (d) and hydrogenation of sample (c) by ion implantation .

The lineshape features are summarised in Table 3.1 together with the hydrogen induced changes. It is apparent that whatever criteria are adopted, pp peak shift, sp shoulder height of L2H shoulder height, the CVD samples show the least change overall and in particular the CVD sample with grown-in hydrogen shows the least change in the L2H component as determined by the high energy shoulder height . Density of states (DOS) determination using the SCLC technique yielded the values shown in Table 3.2. The values obtained for CVD films prepared in our standard manner can be seen to be somewhat higher than desirable for good photovoltaic performance.

Thermal desorption of hydrogen from both GD and CVD films yields results with both high and low temperature desorption peaks in evidence.(Clare *et al* 1987) .Whilst there is no doubt of the presence of hydrogen in the CVD sample, the quantity is small. Infra-red spectroscopy of samples of CVD a-Si:H films yielded definite adsorption peaks due to the monhydride at 630 and 2000 wavenumbers, however, the dihydride signal expected at ≈ 800 wavenumbers is completely obscured by the signal due to surface oxygen. Heating above the first thermal desorption peak has no apparent affect on the monohydride signal. The hydrogen content obtained from the IRS data is low for the CVD samples and somewhat better for the GD sample (Table 3.2).

Samples of CVD films produced by our standard process have been fabricated into Schottky barrier photovoltaic cells by evaporating onto them transparent spots of platinum. These have yielded photovoltages, Voc, up to 430 mv with photocurrents, Jsc, up to 0.4 mA cm^{-2}. Fill factors of 0.3 have been obtained from the J-V characteristics.

3.3 Discussion

The Auger lineshape results are consistent with a low level of hydrogen in our standard CVD films. All the indicators; position of pp component peak, height of the shoulders due to the sp and L2H components, show the hydrogen content in the standard CVD films as less than the ion implanted crystalline and CVD films and also less than the GD films. This is confirmed by TDS and by comparison with the efficiency and fluence values for other workers. DOS information for the standard films are also consistant with the hypothesis of low, probably inadequate levels of hydrogenation and the low Voc, Jsc and fill factors measured.

3.4 Conclusion

We have shown that there is a mutual consistency betweeh the hydrogen content of a-Si:H films and the Auger lineshape, independent of the method of production of the film or the means of incorporation of the hydrogen. Further, it appears that for a-Si:H films produced by APCVD using our standard parameters, there is a

consistency between the techniques we have used measuring the hydrogen coOntent or related parameters. Auger lineshape analysis, DOS by SCLC, IRS and TDS are all predictors of the low hydrogen content. This is confirmed by the present poor performance actually obtained from PV devices fabricated from our films.

TABLE 3.I

Sample	Sample Type	Deposition Temp^r	Sample I.D.	Substrate	Pos^n pp peak	relevant Sh 1	height Sh 2	H_2 content
(c)	CVD	650°	M226	SS	92.8	42	62.5	
(c)	CVD	650°	M226	SS	92.2	49	71.3	
(d)	GD	240-259°C	#611	7059	91.6	42	62	
(d)	GD	240-259°C	#611	7059	90.0	52	73	
(a)	C-Si	240-259°C	SIL 1	C-SILICON	93.0	42.8	65	
(a)	C-Si	240-259°C	SIL 1	C-SILICON	91.5	55.2	77	
(b)	CVD	520°	#518	SS	92.8	37	59	0.5-1.5 at %
(b)	CVD	520°	#518	SS	92.0	44	65	by IR

TABLE 3.2

Sample		H_2 content by IR (2000 cm^{-1}) as deposited	heated >350°C	heated >600°C	H_2 content	DOS
a	C-Si	-	-	-	*4×10^{22} cm^{-3} ≈ 1 at %	-
b	CVD	1.0 at %	1.68 at %	0.85 at %	-	5-10 × 10^{16} eV^{-1} cm^{-3}
c	CVD	-	-	-	*4×10^{22} cm^{-3} ≈ 1 at %	-
d	GD	-	-	-	**1×10^{24} cm^{-3} ≈ 16 at %	-

* ion implanted

** estimated from deposition conditions.

Figure 3.1 AES lineshapes for various a-Si:H samples (see table 3.1 for preparation procedures)

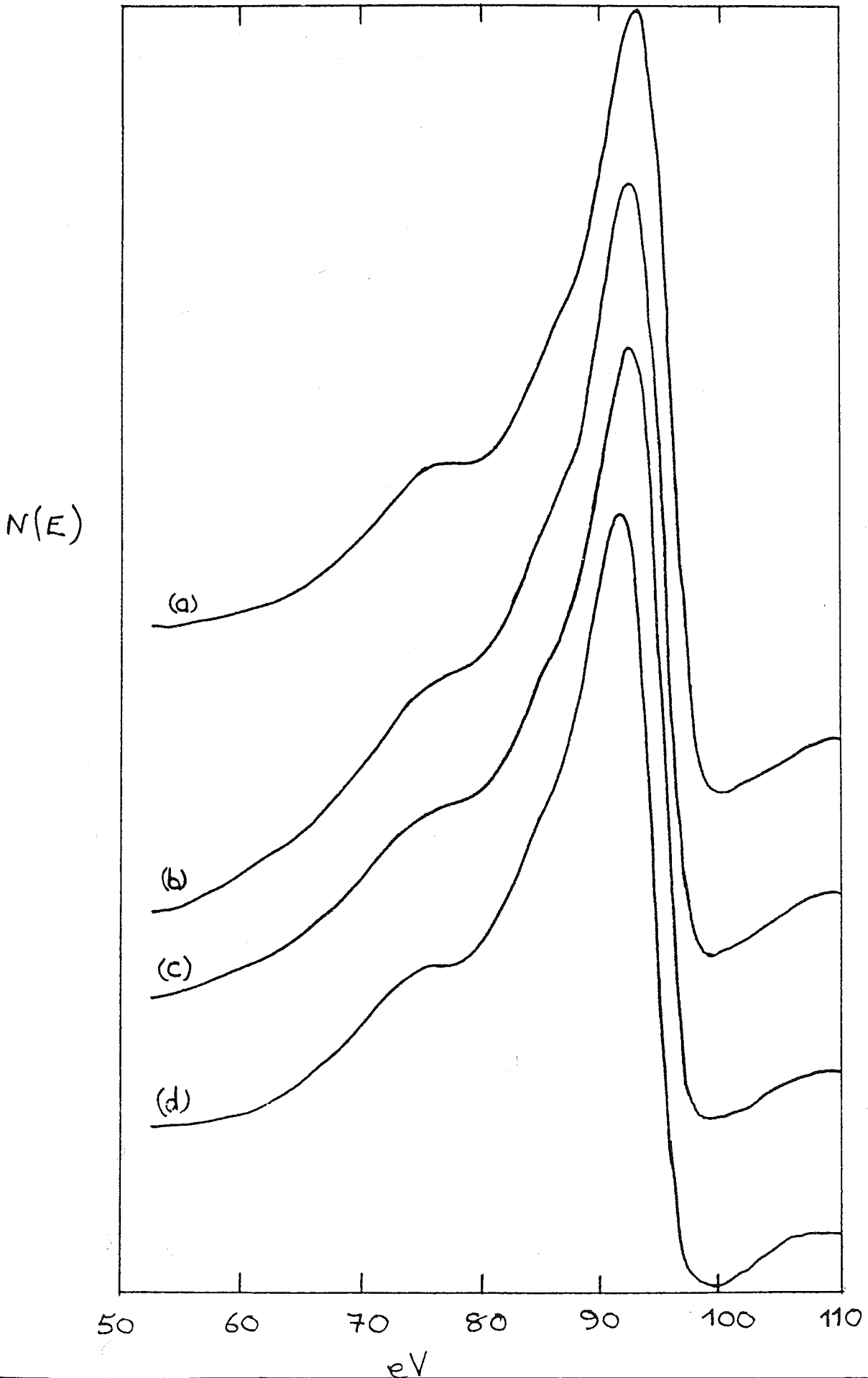

Figure 3.2 AES lineshapes for various a-Si samples

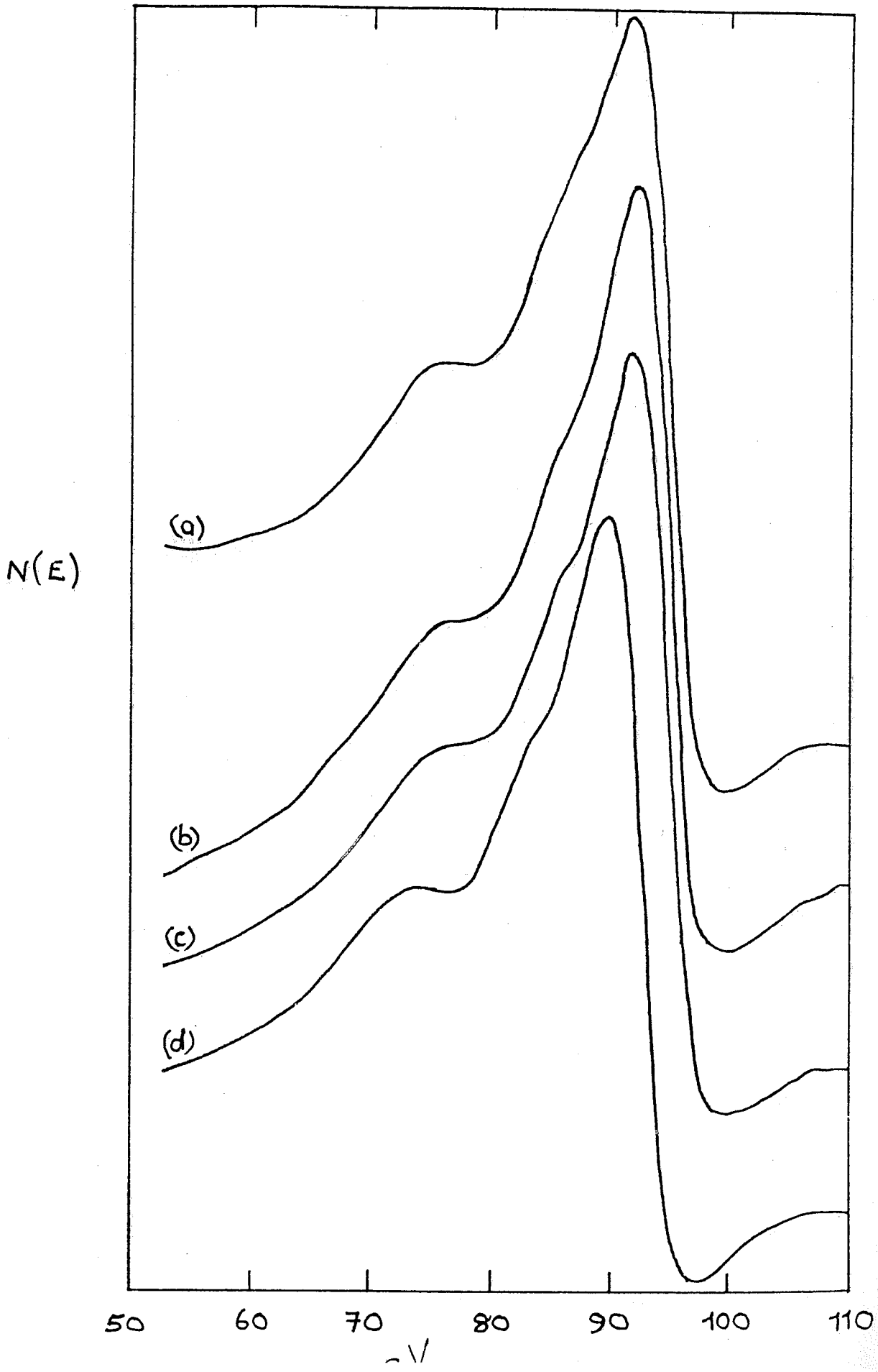

4. CHOICE OF SUBSTRATE FOR AMORPHOUS SILICON SOLAR CELLS

There is considerable difference of opinion in the literature about the best method of preparing stainless steel for use in amorphous silicon solar cells. We have used a chemical vapour deposition (CVD) method to deposit thin films of a-Si:H on various stainless steel surfaces. Our experiments include three commonly-available grades of stainless steel which were prepared in several different ways. The a-Si:H films deposited on these stainless steel substrates were fabricated into Schottky barrier photovoltaic cells and their performance was compared for different substrates and preparation techniques. Considerable differences were found between the performance of the a-Si:H devices prepared on different stainless steel surfaces. The reasons for these differences are explained by performing XPS depth profiling and scanning electron microscopy on the amorphous silicon/substrate interfaces.

As a result of this work we are able to recommend both the most suitable grade of stainless steel to use, and an optimized substrate preparation procedure for amorphous silicon solar cells prepared by CVD.

Amorphous hydrongenated silicon films for photovoltaic applications are generally approximately 500 nm thick. However in the glow discharge process the a-Si:H material is deposited at a rate of only 0.2 - 0.3 nm s^{-1}. Thus a deposition time of about 40 minutes is required for the production of a PV device.

Recently other processes have been reported in which deposition rates of 50-100 nm s^{-1} have been achieved [Ellis and Gordon 1983]. One class of such processes is based on atmospheric pressure chemical vapour deposition of a-Si:H from the higher silanes (e.g. Si_2H_6, Si_3H_6) or from fluorinated silanes [Matsumura and Tachibana 1985]. Some authors have used mercury vapour as a photocatalyst to accelerate the deposition process [Mutsukura, Katoh and Machi 1986]. A considerable amount of research is now in progress to develop and evaluate these new approaches. In general they offer advantages in terms of faster deposition rates, simpler operating conditions and lower energy input during manufacture.

The deposition conditions and the chemical processes involved in CVD are quite different from those which are used for glow discharge. Therefore it is necessary to investigate the optimal choice of substrate for a-Si:H films prepared by CVD. We have confined our attention to stainless steel substrates because of their suitability for continuous, large scale, industrial production of photovoltaic panels.

4.1 Preparation Of Stainless Steel Substrates

The stainless steel substrates were prepared from commercial steel sheet of 0.5 mm thickness. For our purpose the sheet was cut into 10 × 20 mm rectangular pieces which were individually numbered on the reverse side and then attached to a flat plastic forma using double-sided adhesive tape. The following procedure was carried out on the samples.

4.1.1 Polishing. The samples were:

(a) ground flat using course grade (180) silicon carbide paper

(b) progressively polished using four grades of paper (220-4000 grade)

(c) polished to a mirror finish using a cloth and diamond paste (1-3 μm followed by 0-1 μm)

4.1.2 Cleaning and Degreasing. For this stage we followed the procedure of Ellis and Gordon [1983] with a few minor modifications. The samples were:

(a) placed in a stainless steel holder in a beaker of AR isopropanol and heated to just under boiling (i.e. 80°C) for 45 minutes for degreasing.

(b) placed in fresh isopropanol in an ultrasonic bath for 15 minutes

(c) rinsed in ultra pure water

(d) etched in a 1:9 mixture of $HF/HN0_3$ for 10 seconds to remove the remaining oxide layer

(e) rinsed in ultra pure water

(f) rinsed again in isopropanol

(g) rinsed again in ultra pure water

(h) blown dry in a high-purity N_2 gas stream

4.1.3 Passivation: Following this cleaning and degreasing the stainless steel must be passivated for use in the CVD process. Generally this step is not required for GD films because they are deposited at lower temperatures. However, at CVD temperatures, the unpassivated stainless steel can act as a source of contamination of the films (Kurtz, Prozcia and Gordon 1986). Ellis and Gordon (1983) and Kurtz Prozcia and Gordon (1986) and others have suggested various methods of passivating stainless steel and our original approach, based on their recommendations, was to heat the substrates in air on a hot surface at 220°C for twenty minutes and then allow to cool on the hot plate. These substrates were then used in the CVD chamber, as shown in figure 4.1.

4.2 Optimization of Passivation Technique

Our electrical measurements on Schottky diode structures formed on the a-Si:H indicated a high series resistance which we attributed partly to the existence of a thick oxide layer at the substrate a-Si:H junction. XPS depth profiling of this junction showed that oxygen was present in the a-Si:H over a distance of about 60 nm from the metal surface (see Figure 3.2). Some trace element contamination from the stainless steel is also apparent in these depth profiles. It is clear that this passivation technique produces a thick oxide film at the junction. Therefore we attempt to optimize the conditions of passivation of preparing stainless steel samples as in 4.1 and 4.2 above with variations in the passivation temperature and time.

After a considerable number of tests we found that the best PV properties were obtained with substrates which had been allowed to stand in dry air for 12 hours at room temperature prior to film deposition. These substrates had significantly better electrical properties than those which were passivated at higher temperatures or which were allowed to stand in air at room temperature for lesser or larger times. Table 4.1 shows how we optimised the passivation time for 316 stainless steel in dry air at room temperature.

It appears to us that 12 hours passivation in air produces an oxide film of optimal thickness which prevents contamination of the a-Si:H film while also reducing the contact resistance with the substrate to the lowest practicable level.

TABLE 4.1 Effect of Passivation Time on Performance d = 0.7 μm, type = 316 SS

Passivation Time (hrs)	0	3	6	12	24
$\bar{V}_{sc}$ (μA)	55	8	57	116	20
$\bar{V}_{oc}$ (mV)	110	64	135	245	23

Depth profiling of these films indicated that the oxide film produced by this process was about 30 nm thick, as shown in Figure 4.3.

These depth profiles may be compared with those in Figure 4.2 to illustrate the difference in the passivation layer. It is clear that the layers formed at room temperature are thinner than those formed at 220°C. Also, the silicon does not appear to penetrate so far into the passivation layer and thus less of the highly resistive SiO_2 is formed. We used the scanning electron microscope to compare the morphology of oxide films prepared at room temperature and at 220°C and it was clear that the latter were more granular and porous than the former.

4.3 Choice of Variety of Stainless Steel

Stainless steel is available in many different varieties and we have attempted to determine whether any particular type is preferable for PV applications. For this purpose we chose three of the most commonly available grades.

Each of these materials was prepared according to the substrate preparation procedure described above and the passivation times were separately optimized. It was found however that the same passivation procedure was effective for all three varieties of stainless steel (Clare and co-workers 1987).

On the basis of a large number of electrical measurements summarized in Table 4.2, we conclude that there is a substantial difference in performance of a-Si:H films on the three different varieties of stainless steel which we have used as substrates (Clare and co-workers 1987).

TABLE 4.2 Effect of Substrate Choice on Performance d = 0 7μm, 12 hour passivation

Type of Stainless Steel	Composition (%)					Performance	
	Fe	Cr	Ni	Mo	Ti	$\bar{I}_{sc}$(μA)	$\bar{V}_{oc}$(mV)
AISI304	67-75	17-20	8-11	-	-	48	107
AISI316	62-73	16-20	8-14	2-3	-	116	245
AISI 321	70-76	17-20	7-10	-	< 1	19	92

The reason for this difference was was explored by XPS depth profiling of the oxide layers on each of the three varieties. The depth profiles obtained were similar to those reported earlier using Auger depth profiling [Stoddart and Hondros 1972]. All varieties have similar oxide layers on the surface. These layers containing primarily Cr oxide at the surface with an increasing proportion of iron oxide as the metal surface is approached. The Ni and the trace elements Mo and Ti are to be found at greater depth into the material. Thus it is the Fe and Cr oxides which interact with the a-Si:H regardless of the variety of stainless steel used. The main difference between the various grades of stainless steel is the relative thickness of the oxide layers and the permeability of the films. The 304 and 316 grades appear to produce thinner and denser films with the 316 grade films being slightly denser than 304 and thus giving better electrical properties, as shown in Table 4.2.

4.4 Conclusions

We have used electrical measurements and XPS depth profiling to optimize the choice and preparation procedure of stainless steel substrates for a-Si:H thin films, produced by CVD. Our results indicate that

(a) a thin oxide film of approximately 30 nm thickness is desirable to prevent contamination of the a-Si:H. This can be achieved by exposure of the cleaned stainless steel surfaces to dry air for a period of 12 hours prior to deposition.

(b) of the three common varieties of stainless steel (304, 316 and 321), the 316 variety is preferable as a substrate for a-Si:H produced via CVD. We believe that this is due to the better quality of the oxide film produced during passivation of this material.

Figure 4.1 Schematic diagram of apparatus used in this study for atmospheric pressure CVD

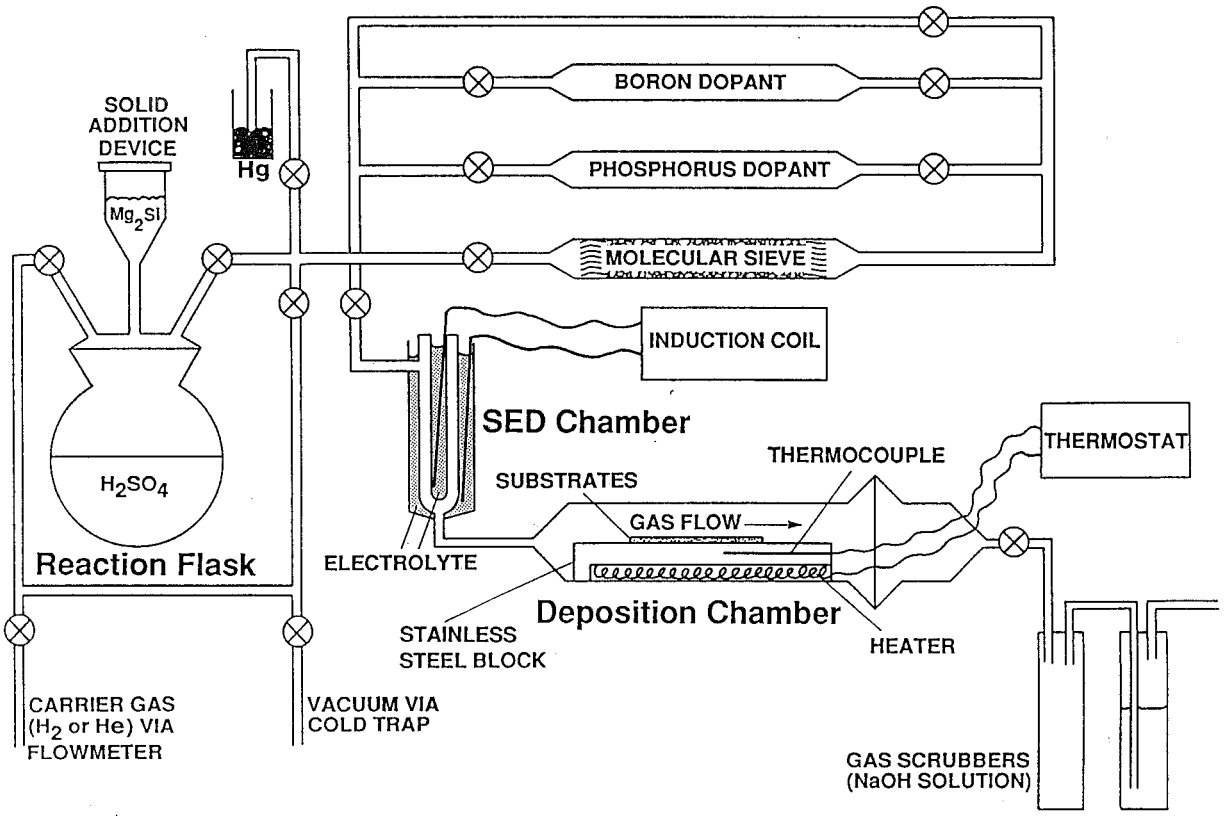

Figure 4.2. XPS depth profiles for a-Si:H on stainless steel for standard method of passivation
1-304 substrate
2-316 substrate

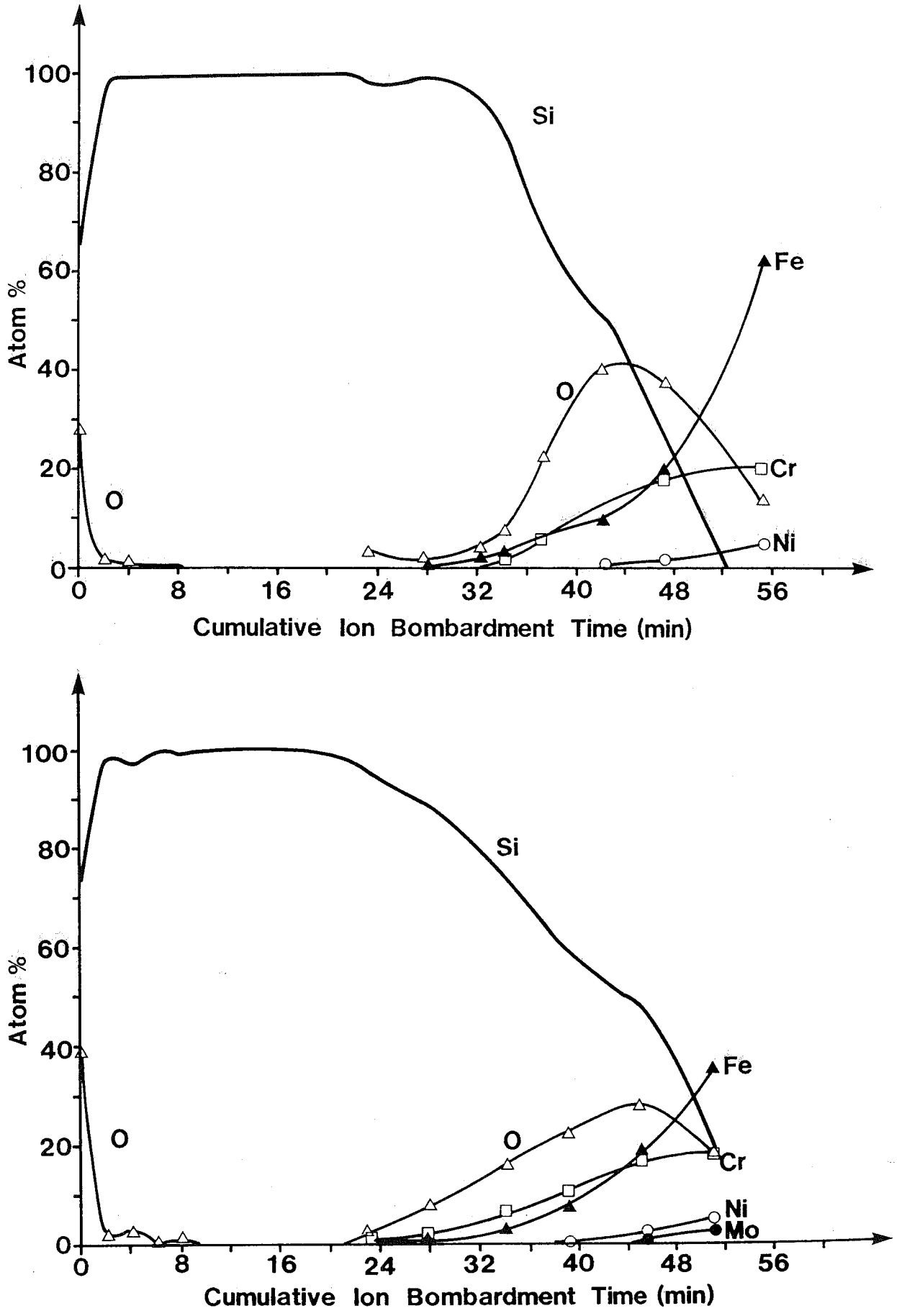

Figure 4.3. XPS depth profiles for a-Si:H on stainless steel for optimal passivation technique.
1-304 substrate
2-316 substrate
3-321 substrate

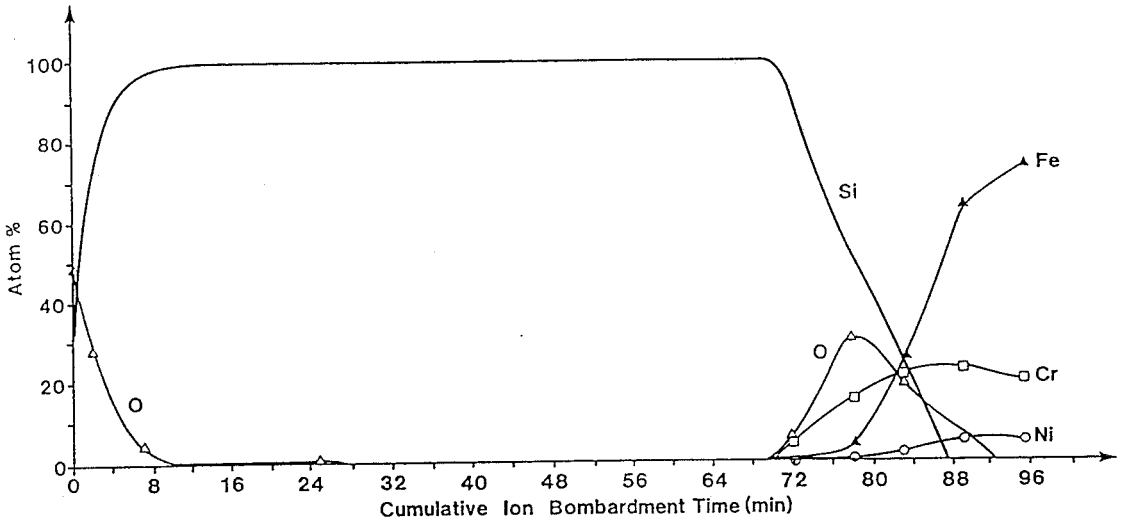

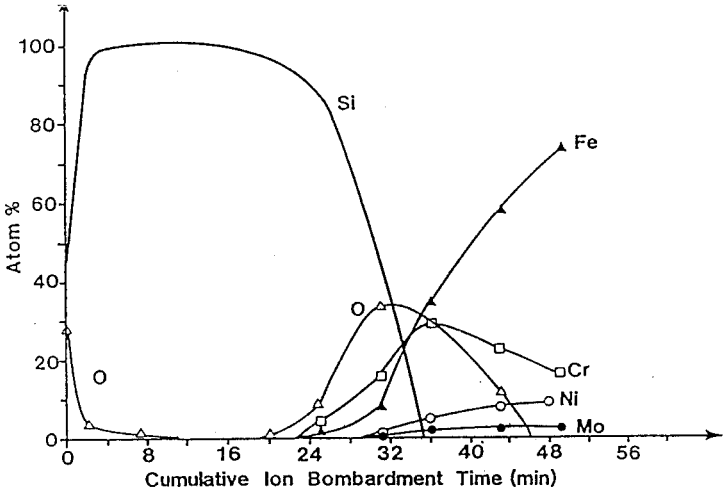

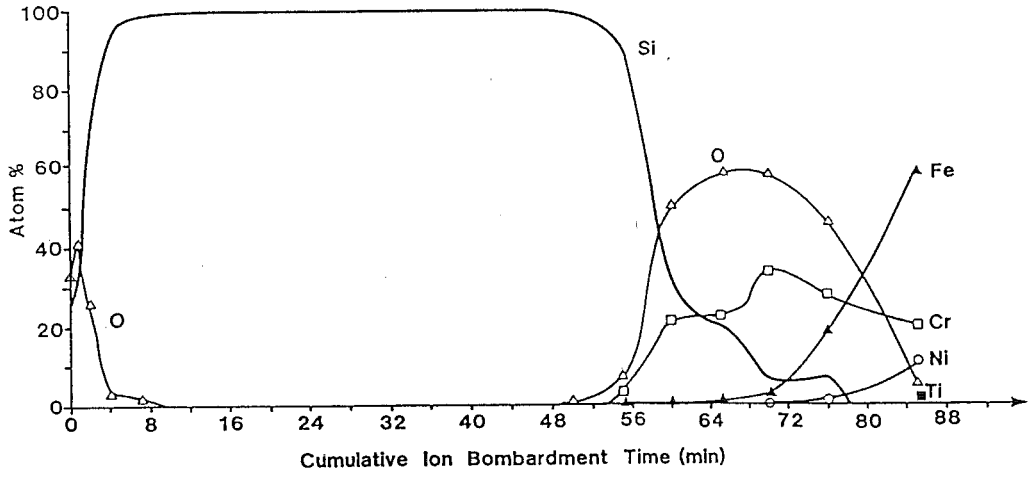

5. DETERMINATION OF THE DENSITY OF GAP STATE BY SCLC METHOD

Although there is a lack of long range order in an amorphous semiconductor, it can still contain defects. Such defects add states in the mobility gap influencing the electronic and optical properties of the material. Thus the density of states (DOS) defined as the number of states per unit volume in a unit energy interval) in amorphous silicon is the key parameter for determining the semiconducting properties of this material. For instance according to Smith and his co-workers (1987), materials with DOS values less than or equal to 10^{16} cm^{-3} produce high efficiency solar cells, while performance is quite poor for DOS values greater than 5×10^{16} cm^{-3}. Hence the determination of accurate DOS value is of considerable importance. There are several methods for determining this.

Spear and LeComber (1972) first developed the Field Effect technique to measure DOS values in a-Si. It measures both bulk and surface or interface states (Powell and Pritchard 1983) and is very sensitive to the possible presence of surface states (Fritzche 1986). Several other techniques such as space charge limited current (SCLC), Deep Level Transient Spectroscopy (DLTS) and Photothermal Deflection Spectroscopy (PDS) have been used to determine the DOS value in a-Sc:H. There is, however, a considerable difference in the measured values and in the distribution of DOS deduced by different techniques. Of course this is not unexpected, because the amorphous state is not a uniquely defined entity and different preparation conditions may lead to different defect structures.

However, among all the techniques SCLC is a classic and reliable technique for the determination of DOS at and just above E_f (the Fermi level). This method was first applied by Den Boer (1981) on GD-samples having n^+-i-n^+ sandwich structure. Recently a number of workers (Bhattacharya *et al* 1982 Mackenzie, LeComber and Spear 1982, , Weisfield 1983, Chek *et al* 1984, Solomon*et al* 1984, Orton *et al* 1984, Gangopadhyay *et al* 1985 and 1987, Yahya and Shanks 1987 and Meaudre and Meaudre 1987) have used SCLC technique to determine the DOS in a-Si:H thin films. In this experiment a non-equilibrium density of charge is injected through the ohmic contact (the cathode) of a thin Schottky diode, which populates the empty gap states above the Fermi level E_f. When the applied voltage is increased, the injected additional charge can extend across the entire sample thickness to the Schottky barrier and the current across the barrier becomes space charge limited. Almost all the charges are trapped but a small fraction is thermally excited to the conduction band and increases the measured current. This bulk enhancement mechanism is analysed to get information about the DOS value above the equilibrium Fermi level. Thus SCLC is extremely simple (the experimental measurements consist simply of determining the current-voltage characteristics for aSchottky barrier diode fabricated from the material of interest) and can potentially yield bulk DOS (all the thickness scaling evidence (Mackenzie *et al* 1982, Bhattacharya *et al* 1982 and Weisfield 1983) indicate that SCLC is a bulk effect) information between the Fermi level and the conduction band.

For the present work, stainless steel (ss)/a-Si/Pt. Schottky barrier cells were prepared for SCLC measurements. In order to calculate the DOS in the gap from the J-V. characteristics, the step by step method of Den Boer (1981) has been

used. in this method, the trap distribution is supposed to be continuous and only slowly varying and also no consideration is given to the distribution of states. According to this method, if the applied potential increases from V_1 to V_2, the quasi-Fermi level moves towards the mobility edge by an amount.

$$\Delta E_f \cong KT \ln\left(\frac{J_2V_1}{J_1V_2}\right),$$

(J_1,V_1) and (J_2,V_2) being two points on the J-V curve, K - the Boltzman constant and T - the temperature in Kelvin. This injected charge condenses within the range ΔE_f and the average DOS within this interval is given by

$$N(E) = 1.5\ \varepsilon_0\varepsilon\ \frac{(V_2 - V_1)}{ed^2\Delta E_f}.$$

Where

ε_0 is the permittivity of free space

ε is the dielectric co-efficient of a-Si:H

e is the electronic charge

and d is the film thickness.

Usually, the point (J_1,V_1) is chosen to be on the ohmic region and (J_2,V_2) is chosen to be on the non-ohmic region of the J-V characteristic in such a way that the value of ΔE_f is several meV.

Figure 5.1 shows the dependence of the density of states (DOS) on film thickness ranging from about 0.1 μm to 1.4 μm for both with and without the use of SED (Silent Electric Discharge) in the system. For film thicknesses less than about 0.98 μm, the DOS increases with decreasing thickness. This occurs probably because the SCLC model does not correct for diffusion currents and because of the effects of the surface and interface layers (Yahya & Shanks 1987). The DOS attains a value of about 10^{17} and remains almost constant with increasing thickness. The saturation in DOS value (above 0.8 μm) arises possibility because the effect of surface and interface layers become negligible as the thickness increases. The high saturation value of DOS ($\approx 10^{17}$ cm^{-3} eV^{-1}) could be attributed to the low amount of hydrogen (not detectable by FTIR) present in our samples.

Figure 5.1 The density of gap states (DOS) as a function of sample thickness.

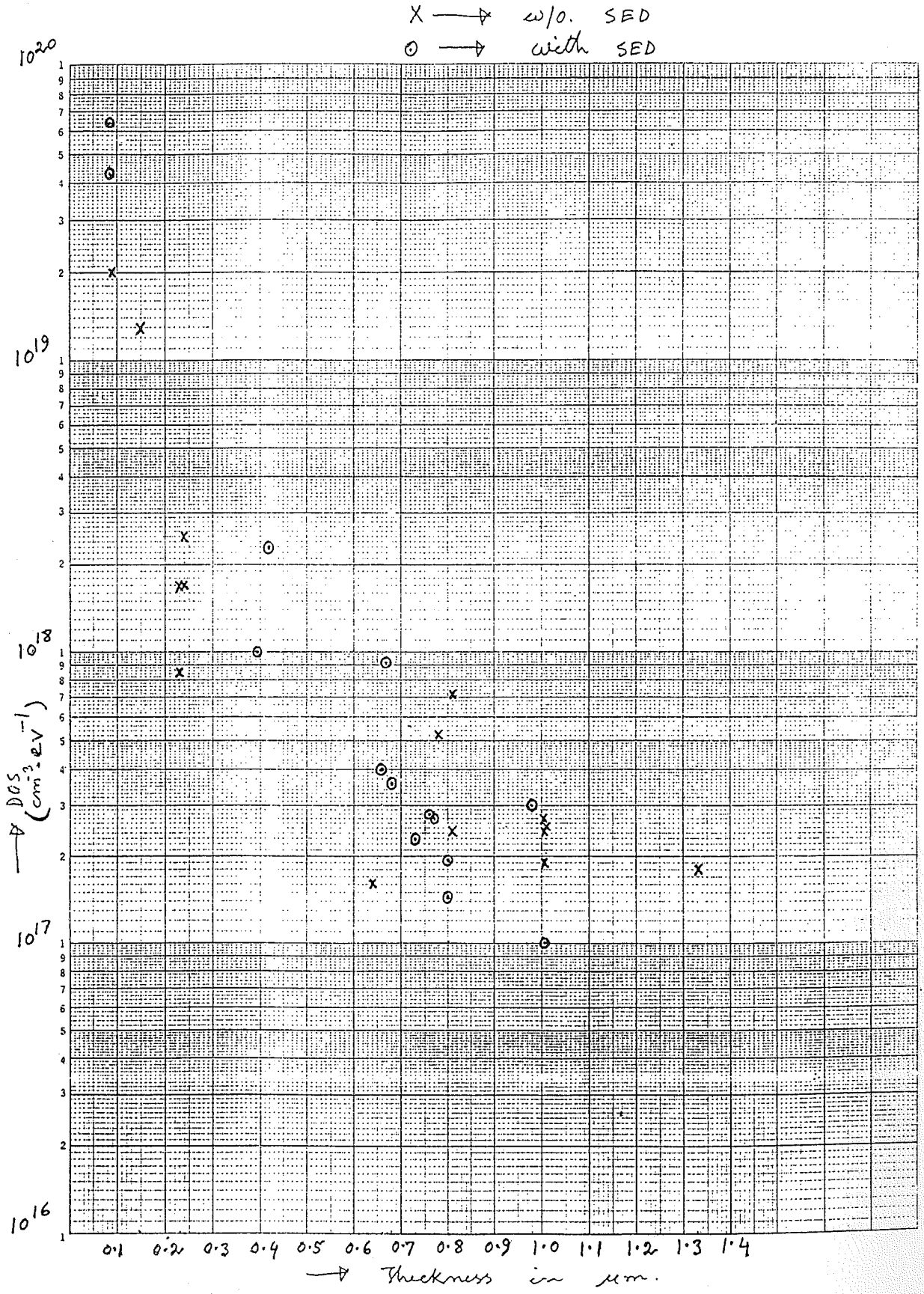

6. MASS SPECTROSCOPY

6.1 Introduction

The current atmospheric CVD system using in situ generation of silanes (Clare *et al* 1987) is not very well characterised. The presence of water vapour, nitrogen or oxygen from leaks, other contaminants from the magnesium silicide/acid reaction, organic solvents from cleaning procedures, all may have an influence on the deposition of hydrogenated amorphous silicon (a-Si:H) and its properties (Corderman and Vanier 1983).

The quantity of silanes produced may vary with different samples of magnesium silicide and different conditions both in total amount and in the ratios of the higher silanes produced. The above factors are susceptible to investigation by mass spectroscopy and in fact several recent studies have been published on the glow discharge decomposition of silane and disilane (Robertson and Gallagher 1986, Gunzel 1985, Longeway, Weakliem and Estes 1984, Longeway, Estes and Weakliem 1984).

The mass spectrometer used by us (VG Masstorr quadrupole mass spectrometer) must be operated in vacuum at a pressure of 10^{-3} millibar of less. The pressure in the CVD system is about 1000 millibars hence a pressure reduction of at least six orders of magnitude is required. This is achieved by a two stage pressure reduction system following the design of Christ *et al*. (1986).

The gas flow is sampled by a capillary tube extending into the gas flow as shown in Figure 6.1. The capillary tube has a length of 3 metres and an internal diameter of 0.2 millimetres and forms the first pressure reduction stage. The low pressure end of the capillary is exhausted by a two stage rotary pump (Edwards E2M 8HS) with a pumping speed of 8.2 m^3h^{-1}. This reduces the pressure at this point to 0.5 - 0.25 millibar, removing the majority of the gas. The pump outlet is routed via a trap containing NaOH to remove the silanes present in the exhaust gas. The pressure at the end of the capillary is still too high for operation of the QMS hence a second stage of pressure reduction consisting of a 50 micron aperture is used. The pressure is thus reduced to 10^{-5} millibar or less above an oil diffusion pump with a LN_2 cold trap. The pressure in the high vacuum part of the system is typically 3 to 5×10^{-6} millibar. The lower detection limit of the QMS with the Faraday collector is 10^{-11} millibar and this allows detection of gas species with a concentration of less than 10 ppm. A simplistic calculation indicated a complete change of gas every second or so. In practice the response of the QMS to changes in the gas composition in the CVD system is somewhat slower than this and is still small, of the order of one minute.

The two stage pressure reduction system is claimed to avoid problems of fractionation of the sampled gas (Christ *et al* 1986) although the effusion process is expected to cause a reduction of sensitivity for gases of increasing molecular weight as the function of $(M)^{-1/2}$ where M is the molecular weight (Yarwood 1967).This corresponds to a correction of about a factor of two over the range of masses from SiH_4 to Si_4H_{10} however the correction for Si_4H_{10} with respect to lower masses is much greater, a further correction is necessary due to the different

Figure 6.1 Schematic of Sampling System

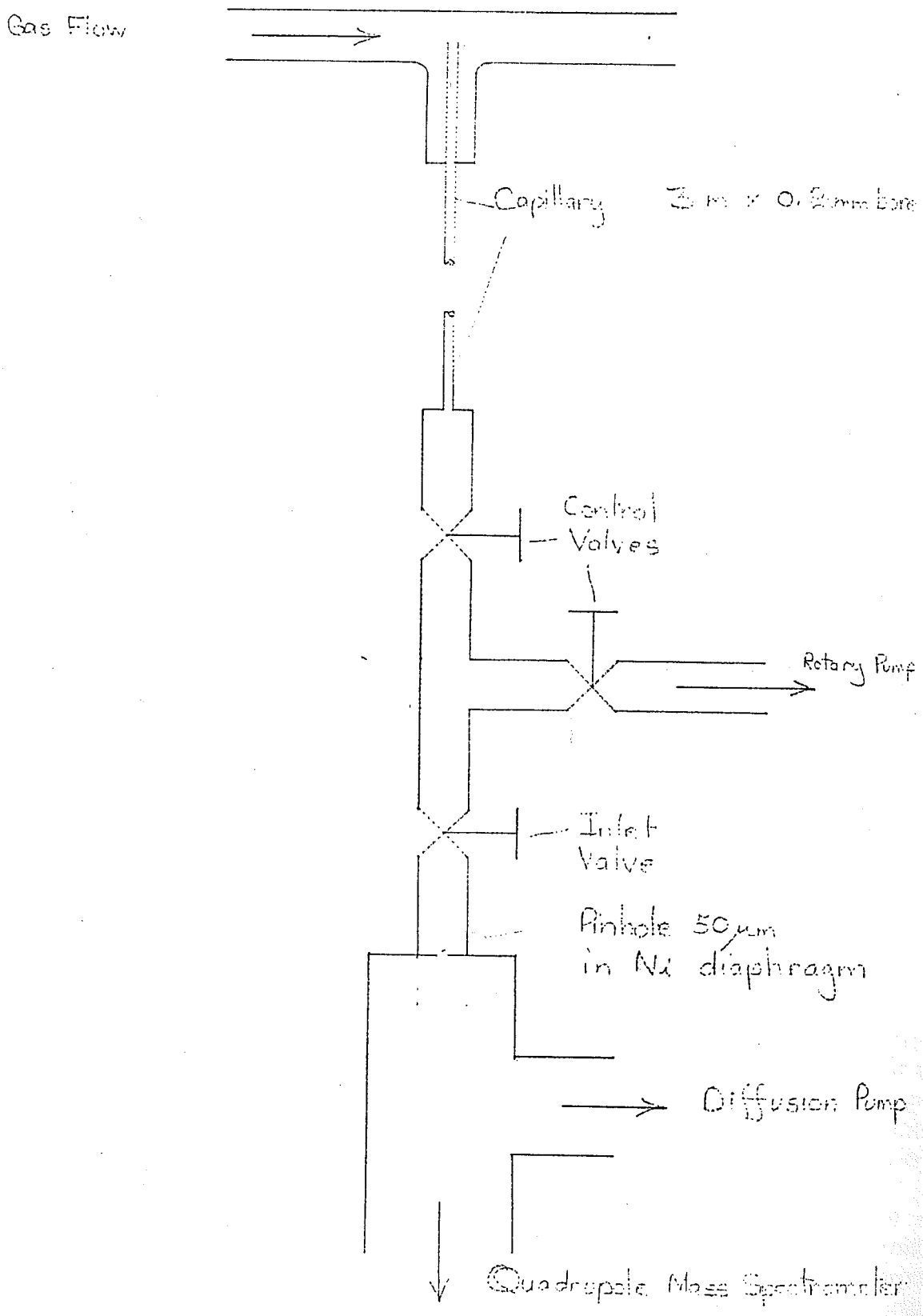

ionisation cross sections and transmission functions of the quadrupole mass filter for the different silane species (Longeway, Estes and Weakliem 1984). Because of these and other uncertainties no correction will be applied to the results at this stage.

A number of experiments have been carried out on the CVD system using the QMS and these will be described below, unfortunately problems with the instrument necessitating its return to the supplier for repair delayed the commencement of this work.

6.2 Residual Gas Analysis

Figure 6.2 shows a series of spectrums obtained of the QMS and CVD systems.

Region a) is the residual gas in the isolated QMS, predominantly hydrogen and water vapour (m/e = 2,18 respectively) characteristic of an unbaked stainless steel system. The peaks at m/e = 28,32,40 are due to nitrogen, oxygen and argon, again as expected, however, the peak at m/e = 43 is unexpected and does not correspond to any commonly found residual gas. The presence of peaks at m/e = 16, 27, 39, 39, 41, 42 and 58 (Hiden 1985) identify the contaminant as acetone. Its origin is uncertain but it is found throughout the system and probably comes from previous cleaning or over enthusiastic leak testing of the system at some stage.

Region b) shows a similar mass range following the QMS being opened to the CVD system, the m/e = 4 peak due to the helium carrier gas has been omitted since this is typically a factor of eight times larger than the peak at m/e = 18. In this region all peaks show an increase in m/e = 28 and 32 possibly indicating a small air leak in the CVD system.

Silane production was then commenced by adding the magnesium silicide to the acid and region c) of Figure 6.2 shows the resultant mass spectrum up to m/e = 34. The increase in pressure due to the silanes requires a reduction in sensitivity as shown. Of note is the SiH_4 spectrum comprising peaks at m/e = 28,29,30,31,32 and 33 (Hiden 1985). Water vapour is still strongly evident though less than the major silane peak and the peak at m/e = 28 is larger than the normal silane spectrum indicating the continued presence of nitrogen.

Region d) is a continuation of c) at higher sensitivity starting at m/e = 34, the acetone spectrum has changed little from b) but a new series of peaks m/e = 56 to 63 has appeared identifiable as disilane (Si_2H_6). Part of the m/e = 58 peak is due to acetone, the major Si_2H_4 peak being at m/e = 60.

Further increases in sensitivity give us region d) where peaks m/e = 84 to 93 are due to trisilane (Si_3H_8) and region e) where peaks m/e = 112 to 123 are due to tetrasilane (Si_4H_{10}). In this region also we see a cluster of peaks m/e = 102 to 109 which may be due to Si_3OH_x where x = 2,3,4,5,6,7,8,9 derived from either the initial reaction or subsequent reactions between the higher silanes and the water vapour present. Higher silanes than tetrasilane may also be present in correspondingly smaller quantities but are undetectable by the present QMS which has an upper limit of m/e = 130.

Figure 6.2 Mass spectrums for Quadrupole mass spectrometer and CVD systems.

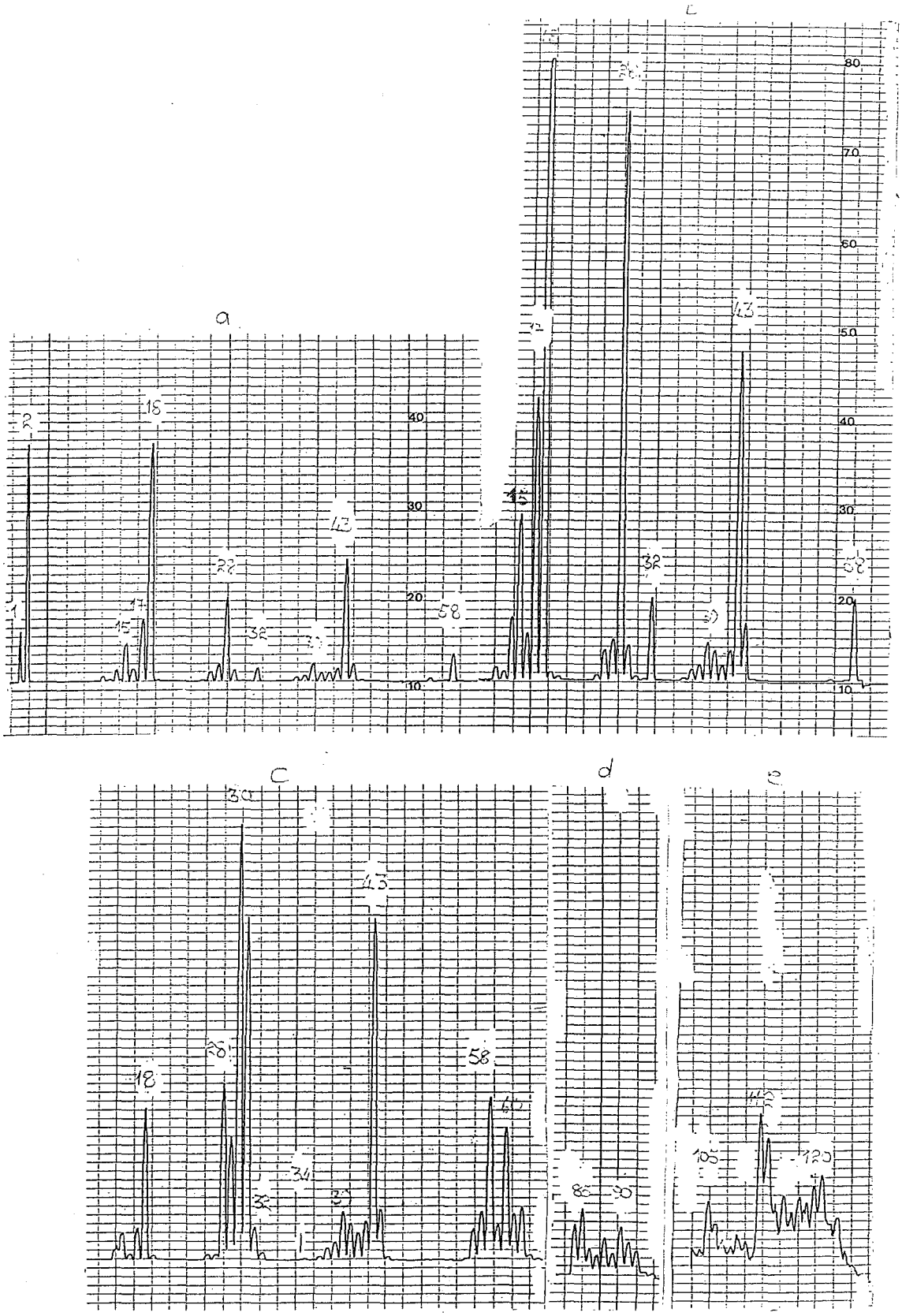

Table 6.1 compares the ratios of silanes produced by other workers with our own measurements. The ratios from our measurements are those of the major peaks observed. It is apparent that even with such a simple procedure our results are reasonably consistent with previous work.

6.3 Effect of Carrier Gas and Silent Electrical Discharge on the Higher Silanes

The silent electrical discharge (SED) has been used to produce higher silanes from SiH_4 feedstock (Spanier and MacDiarmid 1962, Gokhale *et al* 1965) and has been used in our CVD system in an attempt to enhance the proportion of higher silanes with apparent success as determined by resultant deposition rates when the silanes were diluted with He as the carrier gas, but less effect when H_2 was the carrier gas (Clare et al 1987).

The effect of the SED and carrier gas on the higher silanes was tested using the QMS. Two successive depositions were carried out with the QMS open to the CVD system, one with He as the carrier gas and one with H_2 as the carrier gas. During each run the voltage applied to the SED was adjusted by changing the separation of the spark electrodes on the induction coil. The results are shown plotted in Figure 6.3 for the partial pressures of Si_2H_6 and Si_3H_8 as a function of spark length. It is apparent that in both cases the higher silane quantities are reduced rather than enhanced by applying increasing energy to the SED. This appears in conflict with the previous work but it may be that the ratios of the silanes entering the SED is different to the equilibrium ratios and the result is the reduction in the higher silanes ratios to this value. Enhancement of deposition rates found in previous investigations may have been due to other reactions or the production of free radicals not detectable by the QMS. An early experiment for the future is to investigate the effect of our SED on pure SiH_4.

6.4 Influence of Substrate Temperature on Effluent Gases

In this part of the investigation the temperature at which the different components in the feed gas were decomposed was determined by analysing the gas stream after the CVD vessel as function of substrate temperature. The quantities of the three higher silanes as a proportion of the SiH_4 component for an unheated substrate and as a function of substrate temperature are shown plotted in Figure 6.4. The Si_4H_{10} component decreases rapidly with increasing temperature, whereas the Si_3H_8 and Si_2H_6 components decrease slowly with temperature at first, and then rapidly between 550 C and 600 C before appearing to level off at very low values. The temperature scale is too coarse to distinguish between the decomposition temperatures of these latter two species. It is quite clear from the graph that our normal deposition temperature of 525 C or so is in the region where a significant part of the Si_4H_{10} will have decomposed and contributed to the film, but only a small contribution is expected from Si_3H_{10} and Si_4H_{10}. This accounts for the relatively low deposition rates obtained.

Figure 6.3 Partial Pressures of $Si_2:H_6$ and $Si_3:H_8$ as a function of spark length.

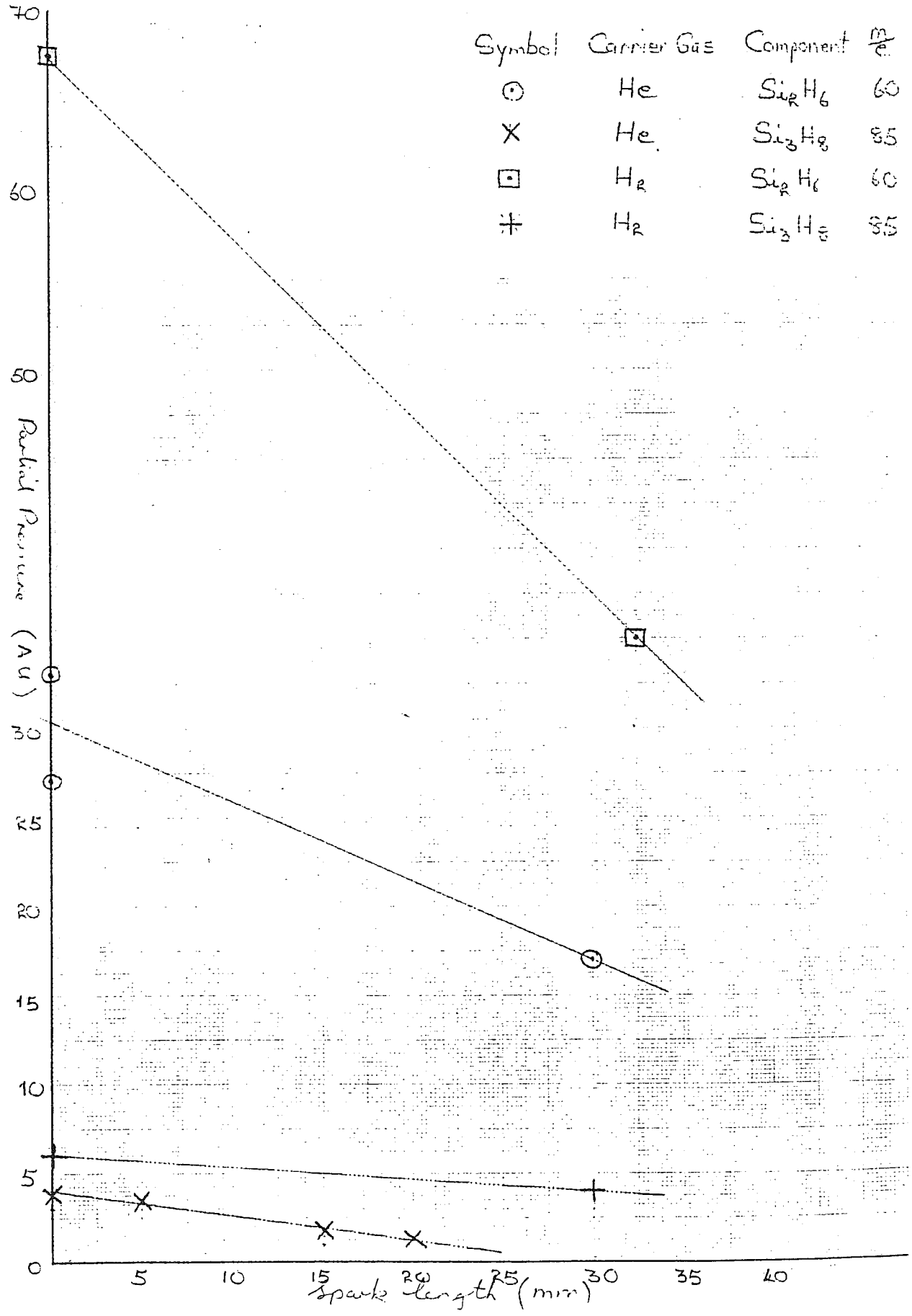

Figure 6.4 Si_2H_6 , Si_3H_8 and Si_4H_{10} relative to SiH_4 as a function of substrate temperature

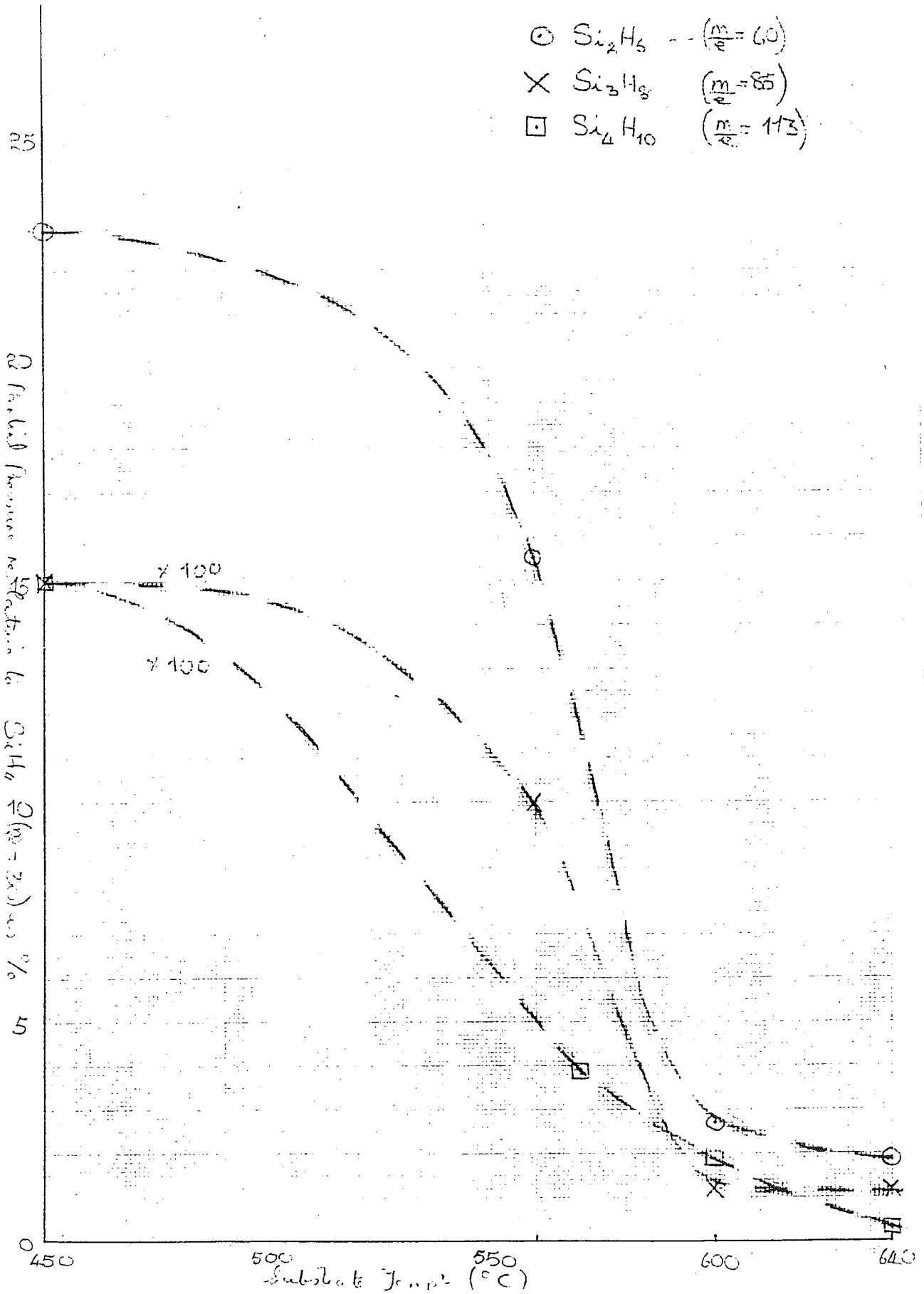

6.5 Effect on the Deposition Process of a Heated Tungsten Filament Adjacent to Substrate Surface.

In this investigation we used at tungsten filament as shown in figure 6.5 to ionise the hydrogen carrier gas. The substrate temperature was set at 425° C to avoid purely thermal decomposition of the silanes on the substrate. The partial pressures of SiH_4 and Si_3H_8 in the effluent gas were monitored with the QMS for a range of filament temperatures.

With the filament cold, no film deposition was observed on the substrate, as the temperature of the filament was increased a powdery deposit appeared on the substrate immediately downstream from the filament. On increasing the temperature further the filament could be seen to be getting thicker in the heated region due to deposition of silicon on the filament itself and a plume of silicon dust appeared with the filament as its source due to decomposition of the silanes close to it. The graph in figure 6.6 show the partial pressures of SiH_4 and Si_3H_8 as a function of the voltage applied to the filament. Clearly, as the temperature of the filament increases more of the silanes are decomposed and lost from the gas stream. After approximately one hour the deposit observed on the substrate was still very thin (showing the first order blue fringe). The filament diameter had increased from 0.2 mm to about 1.0 mm. The experiment gave predictable results since at the high pressure (approximately atmospheric) the mean free path of the H^+ would be too short to influence reactions at the substrate surface and only gas phase reactions would occur. For the same reason it would not be possible to distinguish between reactions due H^+ and purely thermal effects.

An experiment indicated for the future is to repeat the procedure with a system pressure very much lower so that the mean free path of the ions is of the same order as the dimensions of the CVD tube.

Figure 6 .5 View of substrate block set up for filament experiment.

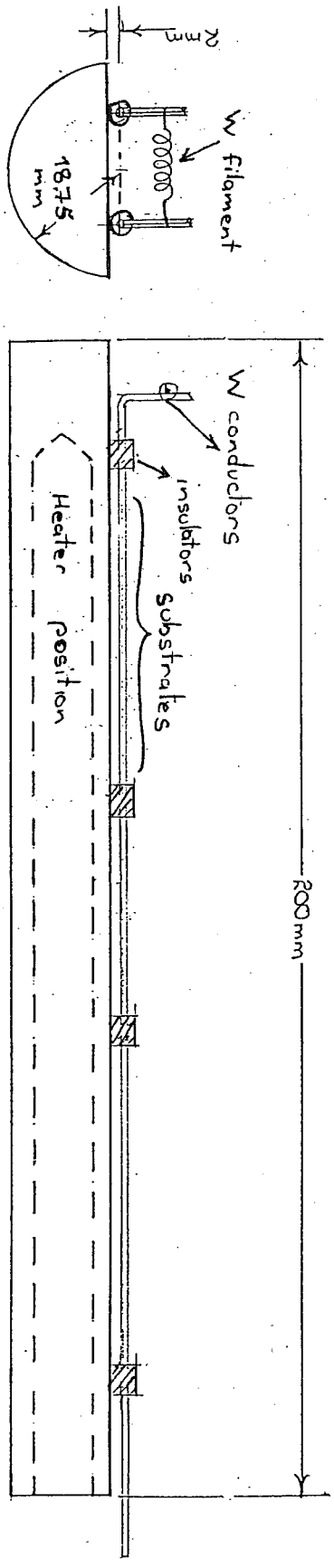

Figure 6.6 Partial pressures of SiH_4 and Si_3H_8 as a function of voltage applied to the filament

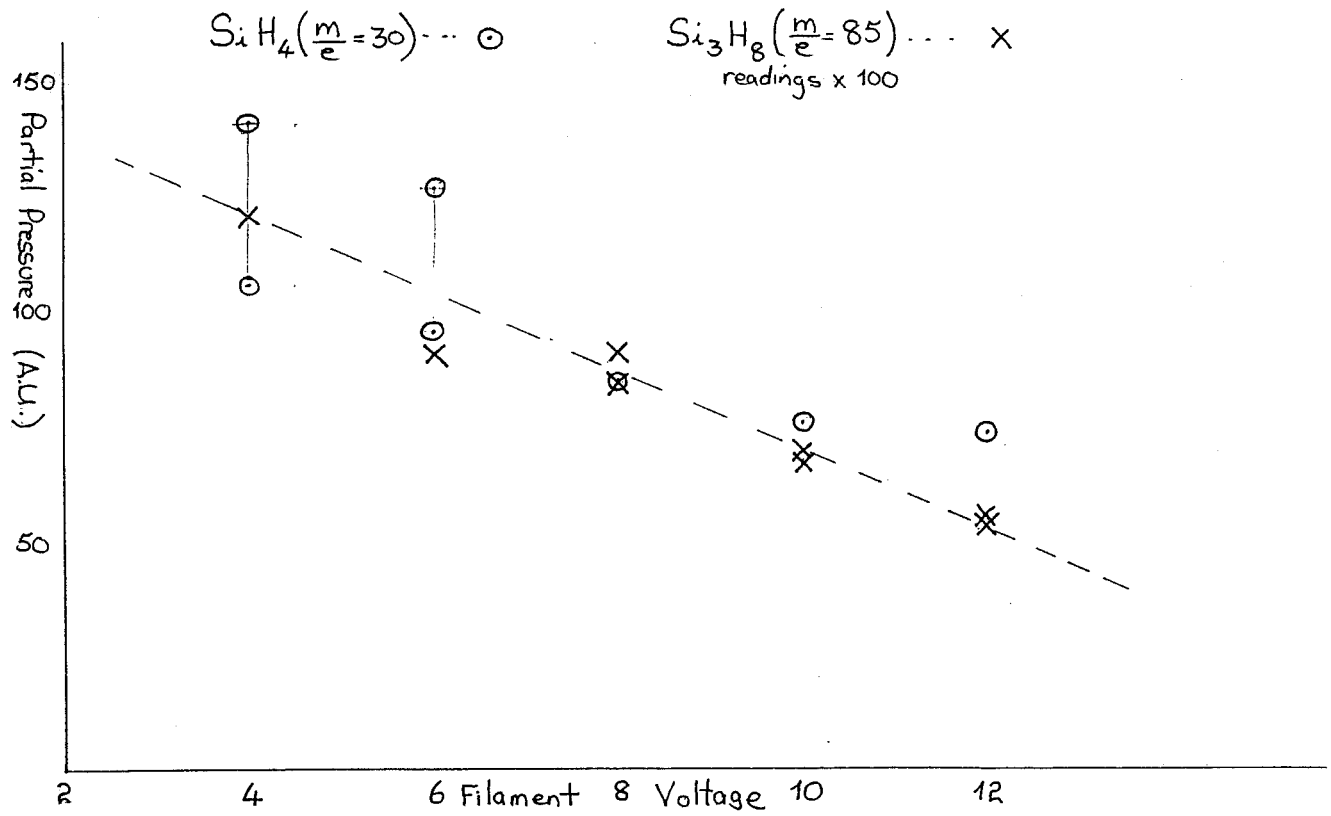

TABLE 6.1

SPECIES	YIELD		YIELD		YIELD
SiH_4	49	(100)	4	(100)	100
Si_2H_6	23	(47)	2	(50)	54
Si_3H_8	5.7	(11.6)	1	(25)	4.6
Si_4H_{10}	0.8	(1.6)	0.25	(8)	0.5 - 7.0
TECHNIQUE	MODULATED MASS SPECTROSCOPY		GAS CHROMOTOGRAPHY		MASS SPECTROSCOPY
PROCESS	Mg_2Si/HCl/HF		Mg_2/HCl/HF		Mg_2Si/H_2SO_4
REFERENCE	1		1		This work

1 KURTZ, PROSCIA and GORDON (1986)

7. INFRA-RED SPECTROSCOPY

Steven Phillips (1986) has shown that the technique of infra-red vibrational spectroscopy can give useful information on factors important to the performance of our APCVD samples as photovoltaic cells. The main piece of information the IR vibrational spectrum can tell us is the estimated atomic hydrogen content C_H. It can also show the existence of impurities if they are in sufficient quantity (generally > at... %) and can lead to assumptions about the hydrogen bonding arrangements.

In his study, detailed analysis of the vibrational spectra of films deposited using APCVD were described on a limited number of very thick films grown on crystalline silicon substrates. Subsequent studies have been undertaken to further develop these techniques and to apply them to thin (0.1 to 0.7 μm) samples. Comparisons with RF sputtered a-Si and a-Si:H samples as well as glow discharge a-Si:C:H samples have also been undertaken. Exploratory experiments similar to those of Biegelson (1979) and Smith and Strongin (1981) have been performed to study the hydrogen bonding configurations in our APCVD samples. These results are presented.

7.1 RF Sputtered and APCVD a-Si:H

During his investigations Steven Phillips initially made measurements on films deposited on stainless steel (reflectance) and crystalline silicon substrates (transmission). Samples on stainless steel were quickly abandoned in favor of c-Si substrates because strong interference fringes were destroying the small signal received. Initial measurements of samples on crystalline silicon 1.2 to 1.4 μm produced strong interference and some slight structure. In an attempt to reduce the effect of the interference and to increase the signal resolution, substantially thicker films were grown and analysed. Interference fringes were completely absent from the resulting spectra. Furthermore good structure and higher signal to noise were achieved.

For the reasons mentioned above it was initially believed that attempts to measure the vibrational spectral of RF sputtered samples of 0.7 μm or less would be unsuccessful. A plot of a typical vibrational spectrum for a RF sputtered a-Si:H sample (0.7 μm thick) with a hydrogen content of ~ 20 at .% is shown in figure 7.1. This can be compared with figure 7.2 which shows a typical APCVD sample (9-12 μm thick) with a hydrogen content of ~ 0.8 - 1.5 at.%.

As can be seen in figure 7.1 there is no evidence of strong interference fringes and there is distinct structure visible in the spectrum. This clearly suggests that it is possible to perform IR studies on films between 0.4 and 0.7 μm in transmittance. Although no confirmatory experiments have been performed due to the unavailability of samples it would appear possible to perform such studies on APCVD samples of similar thickness. This has several advantages. Firstly there is no need for the multiple depositions required for thicker samples and therefore the inherent problems associated with those samples. Secondly samples of this thickness would more closely resemble the standard stainless steel samples used

Figure 7.1 IR spectrum for a Si:H sample prepared by sputtering.

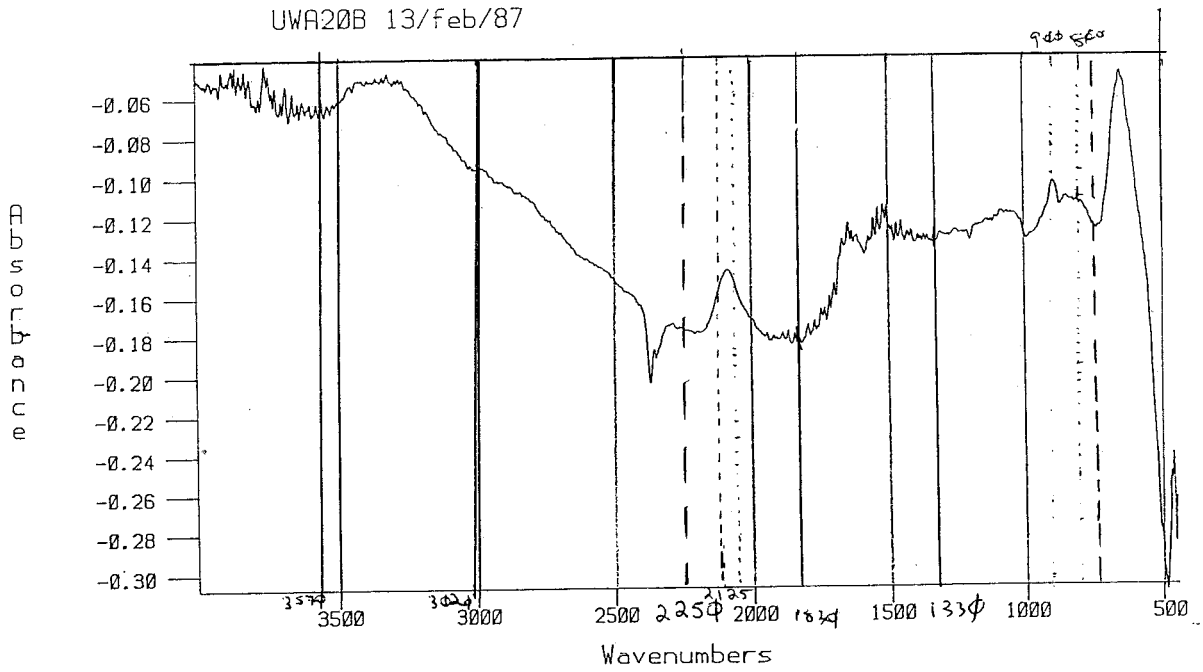

Figure 7.2 IR spectrum for a-Si:H

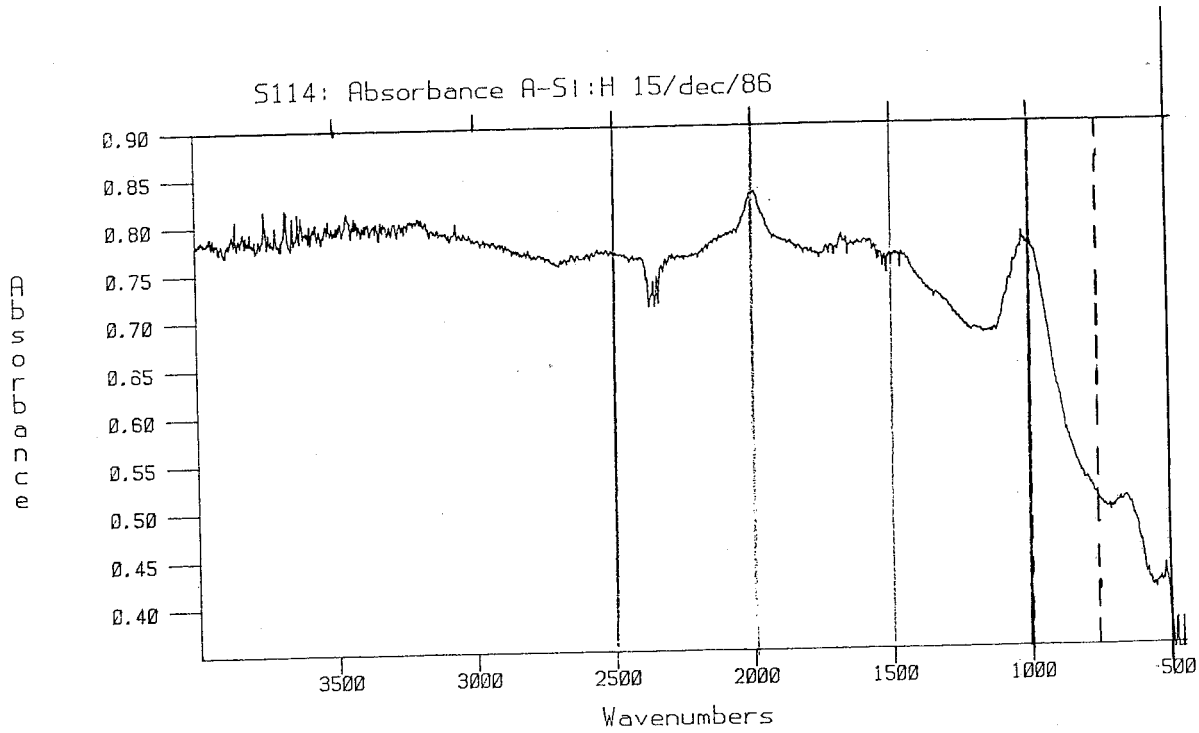

for electrical testing and have the advantage of being easily produced in the same deposition, for better comparison. Thirdly this is the optimum thickness range for photovoltaic properties.

The inherent disadvantage is that some resolution is lost at these thicknesses, especially for those samples with a low hydrogen content. As our samples often contain low hydrogen contents there may be some loss in accuracy or the hydrogen associated peaks may not be visible. As shown, however, there appear to be few problems with this technique at the 10-20 at % hydrogen levels seen in the RF sputtered samples. Further investigation is needed to determine whether it can be applied to APCVD samples of this thickness, especially those with low hydrogen contents, however the above results show this to be promising.

The main features of the APCVD (figure 7.2) are:-

1. a strong Si-H stretching mode at 1990 cm^{-1};
2. A series of three small absorptions on a weak broad peak that stretches between ~1800 and 1450 cm^{-1} ;
3. a broad oxygen absorption peak stretching from 1200 to 900 cm^{-1} ;
4. no clear evidence of Si-H bending modes from 850-900 cm^{-1} due to the apparent convolution with the oxygen absorption mode;
5. evidence of the Si-H wagging mode at ~ 650 cm^{-1} but it is convoluted with the oxygen peak.

The oxygen peak in figure 7.2 appears to be diminished when compared to that obtained by Steven Phillips in his work. This would suggest that with greater technical care it should be possible to significantly reduce the oxygen content in thick multiple deposition samples thereby enabling the possible use of the 600 cm^{-1} for more accurate determination of the hydrogen content.

Figure 7.1 on the otherhand although similar, has significant differences:-

1. the strong Si-H stretching mode has shifted by ~ 80 cm^{-1} to 2070 cm^{-1}. This corresponds closely with the results of Freeman and Paul (1978);
2. no sign of a broad oxygen absorption peak stretching from 1200 to 900 cm^{-1} ;
3. because there is no oxygen Si-H bending modes are clearly visible from 850 - 900 cm^{-1} ;
4. a strong Si-H wagging mode at ~ 650 cm^{-1} which has no convolution with other peaks and is therefore ideal for hydrogen content determination.
5. A broad peak stretching from ~ 3570 to ~ 3020 cm^{-1} .
6. Two absorption peaks on a weak broader peak that stretches from ~ 1830 - ~1330 cm^{-1} .

This is in good agreement with the work of Freeman and Paul (1978).

7.2 APCVD High Temperature Samples

As part of the Auger lineshape experiments of section ... several high temperature APCVD samples were deposited in an attempt to make hydrogen free a-Si APCVD samples. In order to determine the success, or otherwise, of this method for preparing hydrogen free samples, and as a comparison with samples prepared normally, IR transmission spectra were obtained.

The samples themselves were prepared on crystalline silicon substrates at a substrate temperature of 650°C (actual) and allowed to cool in He to ensure no hydrogen was incorporated into the Si network. It is well known [Zhong-tao *et al* 1985] that hydrogen effuses from a-Si:H samples at temperatures above 600° C, and by cooling in He instead of H_2, as normally done, it was hoped to prevent hydrogen being incorporated back into the lattice.

These IR spectra as well as determining the hydrogen content for the Auger studies also serve as comparisons with RF sputtered a-Si and normal APCVD a-Si:H samples.

Figure 7.3 shows a typical absorption spectra for the samples prepared at high temperature. The main features of this spectra are:-

1. a weak Si-H stretching mode at 1990 cm^{-1} , similar to that in the APCVD a-Si:H samples;

2. a series of three small absorptions on a broad peak that stretches between $\tilde{}$ 1800 and 1400 cm^{-1};

3. two strong, broad, peaks, each with considerable interference above it between $\tilde{}$1300 and 400 cm^{-1};

4. no clear evidence of the existence of the broad oxygen absorption peak stretching from $\tilde{}$ 1200 to 900 cm^{-1} found in previous APCVD a-Si:H samples, or the Si-H bonding modes from $\tilde{}$900 to 850 cm^{-1} , due to the interference;

5. no evidence of the Si-H wagging mode at $\tilde{}$ 650 cm^{-1}, seen in previous APCVD samples, again because of the interference. Therefore it is not possible to use this peak as a means of calculating the hydrogen content.

Attempts to integrate under the 2000 cm^{-1} peak of the high temperature samples proved impossible due to the low signal to noise ratio in this region. This tends to suggest that the incorporated hydrogen content is very low.

Hydrogen desorption experiments similar to those of Zhong - Tao *et al* (1985) were performed in conjunction with the IR studies (a more detailed report on this experimental technique is given later in this section). The desorption spectrum was typical of APCVD a-Si samples. There appeared to be some difference in the peak areas, however, with the high temperature samples having much smaller areas. The peak corresponding to the first stage of hydrogen was diminished when compared to the corresponding peak on a similar a-Si:H sample with 0.8 to 1.5 at.% hydrogen. Peak two (corresponding to the second stage of hydrogen)

Figure 7.3 IR Spectrum for a-Si:H sample prepared by APCVD at high temperature

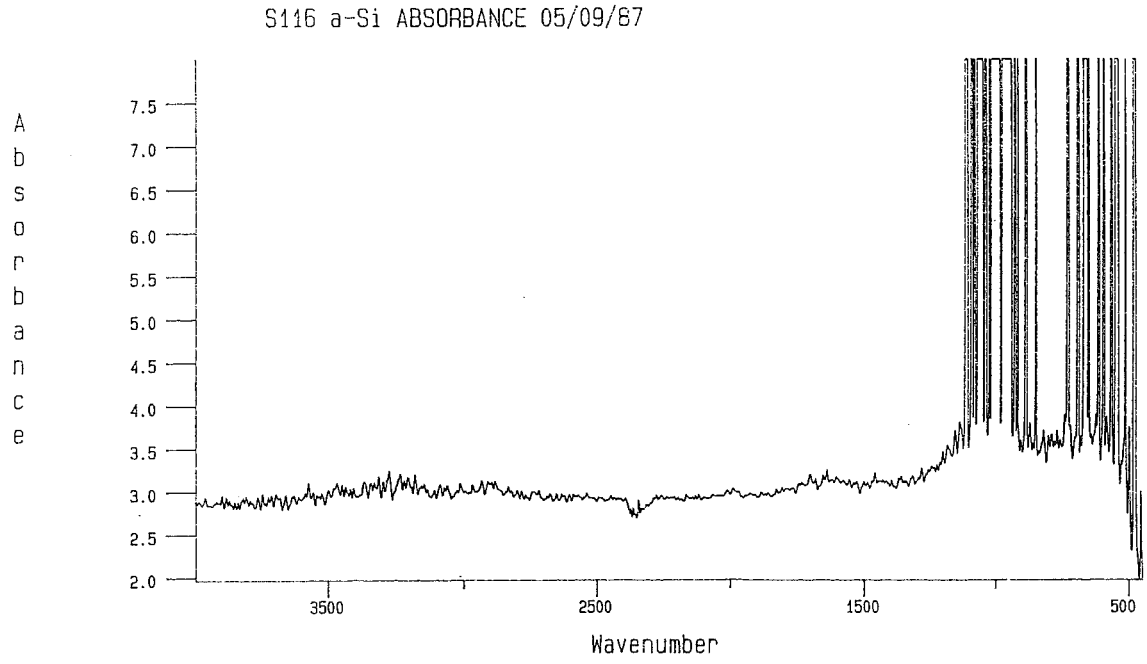

Figure 7.4 IR spectrum for a-Si:H sample prepared by GD

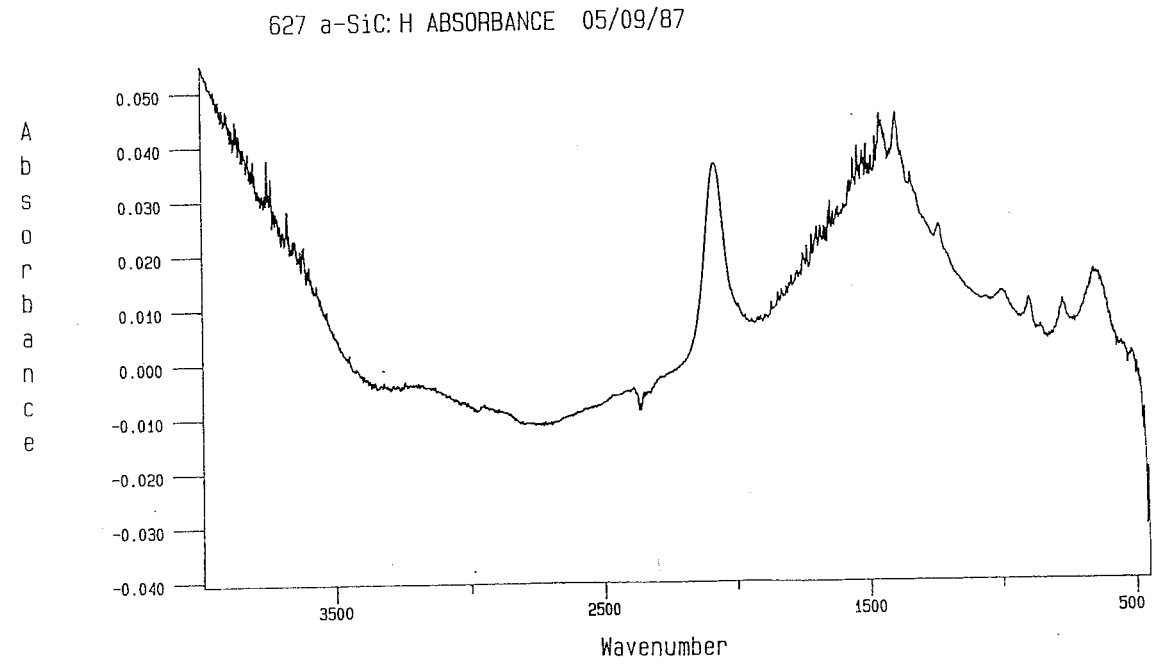

Figure 7.5

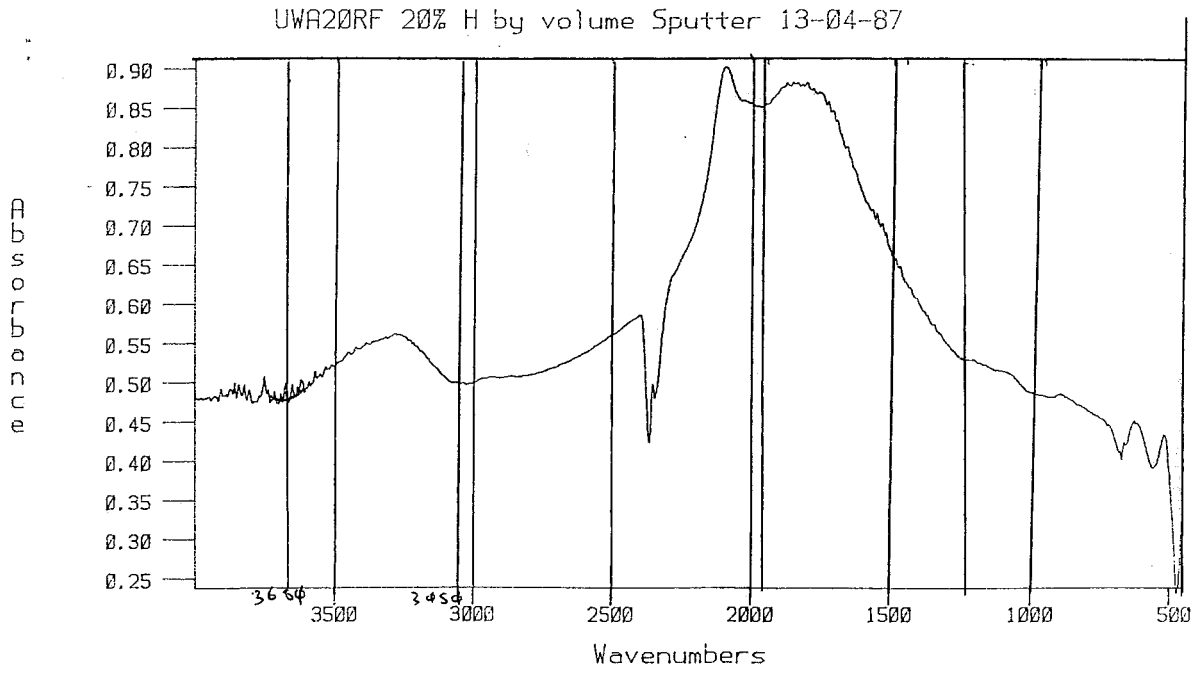

Figure 7.6

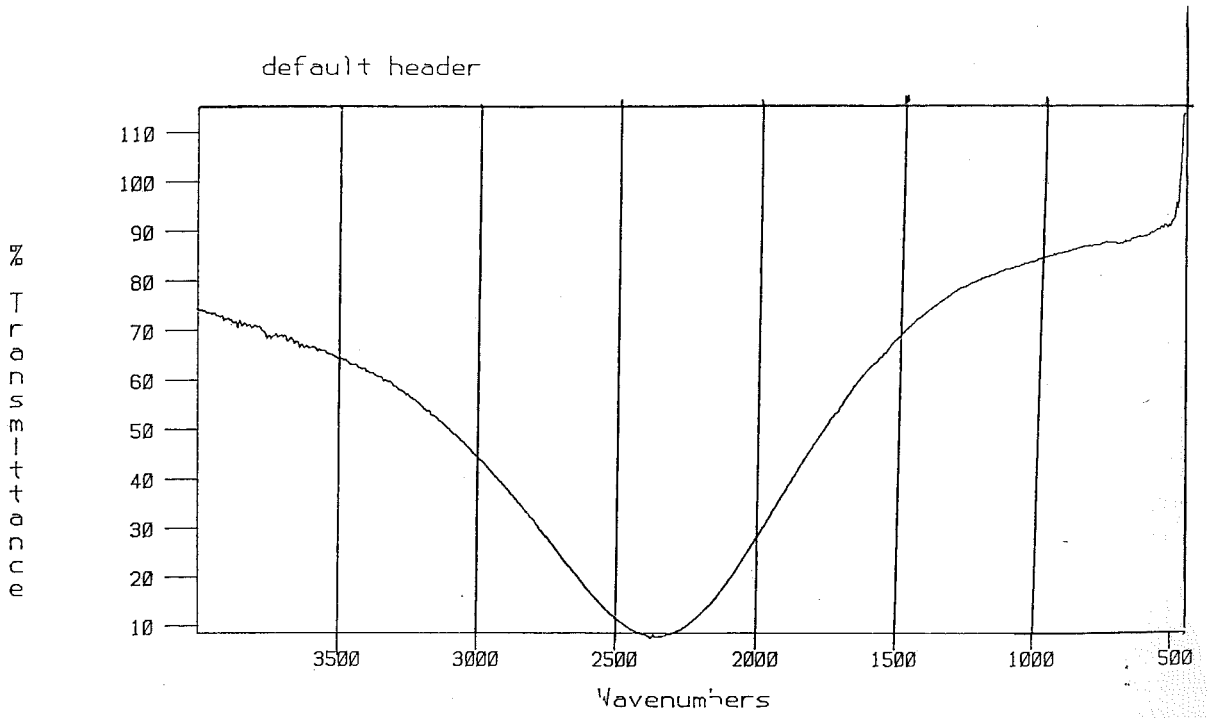

was also diminished when compared to the second peak in the similar a-Si:H sample, but was proportionally larger than its own first peak.

Although not clear cut, the infrared and thermal desorption experiments together give an indication of the hydrogen content of the high temperature films. Both show that the sample does contain some hydrogen despite the precautions taken to exclude it, although that amount is very small and much lower than that of the normal APCVD a-Si:H samples (0.8-1.5 at.%).

7.3 Glow Discharge a-Si:C:H Sample

Figure 7.4 shows a typical absorption spectra for a glow discharge a-Si_{1-x} C_x:H sample (no. 627) where x = 0.3, analyzed in reflectance mode. The main features of this spectra are:-

1. a strong Si-H stretching mode at ~ 2110 cm^{-1}, a shift of about 120 cm^{-1} when compared to that of APCVD a-Si:H samples;

2. a strong, broad, absorption peak stretching from ~1950 to 1100 cm^{-1}. This peak is very much stronger and sharper than the one visible in the APCVD a-Si:H samples. It also lacks the series of three superimposed peaks distinctive of the APCVD a-Si:H samples.

3. a series of smaller, sharp peaks between approximately 1100 and 700 cm^{-1};

4. clear evidence of a Si-H wagging mode at ~ 650 cm^{-1}. It has the distinctive advantage of not being convoluted with any surrounding peaks and will therefore be the most reliable means of calculating the hydrogen content (Shanks *et al* 1980).

This spectrum shows several distinctly different features to those of the APCVD a-Si:H samples, and these can be attributed to the carbon incorporation within the lattice (Saraie *et al* 1984) The glow discharge a-$Si_{0.7}C_{0.3}$:H sample does, however, still show the clear Si-H stretching and wagging modes. From these two peaks it was relatively simple to calculate the hydrogen content attached to the silicon. The other peaks would also, no doubt yield the concentration of hydrogen attached to carbon atoms, however this has yet to be done for this sample.

7.4 Infra-red Reflectance Spectroscopy of a-Si:H

As well as transmittance IR spectroscopy using crystalline silicon substrates attempts have been made to apply reflectance IR spectroscopy to samples with a stainless steel substrate. The technique used was similar to that used by Phillips (1986) in his initial experiments. A plot of a typical vibrational spectrum, taken in reflectance, for a RF sputtered a-Si:H sample (0.7 m thick) with a hydrogen content of ~20 at.% is shown in figure 7.5.

Figure 7.5 bears a good resemblance to that of the transmittance sample in figure 7.1:-

1. A broad peak in the transmittance spectrum.

2. The strong Si-H stretching mode is visible at ~2070 cm^{-1} as in figure 7.1, however it is convoluted on the lower wavenumber side with a strong peak adjacent.

3. A strong broad peak stretching from ~1970 - 1250 cm^{-1} which does not appear in the transmittance spectra. It does however appear in all of the GD reflectance spectra taken. The cause of the peak and why it appears in the reflectance, but not the transmission, spectra is not yet known.

4. No sign of the two peaks on the weak broader peak between ~1830 and ~1320 cm^{-1} due to the presence of the strong broad peak mentioned above.

5. Faint Si-H bending modes are visible from ~850-900 cm^{-1} , however they are not as strong or distinct as those in the transmission spectrum;

6. a strong Si-H wagging mode at ~ 650 cm^{-1} with no convolution with other peaks, as seen in the transmission spectra, and therefore ideal for hydrogen content determination.

As can be seen in figure 7.5 there is no evidence of the strong interference fringes noticed by Phillips and there is distinct structure visible in the reflectance spectrum of figure 7.5. This clearly suggests that it is possible to perform reflectance IR studies on a-Si:H films between ~0.4 and 0.7 m thick. Furthermore as shown above these spectra show good agreement with the spectra obtained using reflectance. Figure 7.5 has also shown that the A-Si:H wagging mode at 650 cm_{-1} is clearly visible and therefore, with minor changes to the equation used for transmission, that the hydrogen content can be determined reasonably accurately. This has the advantage that the actual samples used in subsequent experiments (eg. photovoltaic, AES or optical) can be analyzed non destructively and the hydrogen content and bonding determined.

Again the inherent disadvantage is that some resolution maybe lost at these thicknesses, especially for those samples with a low hydrogen content. As shown, however, there appear to be few problems with this technique at the 10-20 at...% hydrogen levels seen in the RF sputtered samples.

Figure 7.6 shows a typical APCVD sample (0.8 m thick) with a hydrogen content of ~ 0.8 to 1.5 at...% measured in reflectance. It is seen that this sample suffers from the problems with interference fringes similar to those tested by Phillips. As before there is no visible structure. No further confirmatory experiments have been performed due to the unavailability of samples. Further investigation is needed to determine whether it is possible to apply this technique to APCVD samples in the thickness range ~0.4 - ~0.7 m, especially those with low hydrogen contents. The results of the RF sputtered samples, however, show this to be a promising avenue.

7.5 Hydrogen Desorption and IR Spectroscopy

Exploratory experiments similar to those of O.K. Biegelsen *et al* (1979) and Smith and Strongin (1981) were performed to study the changes in the infra-red spectrum of our APCVD samples as the various stages of hydrogen were

outgassed. The outgassing was done using a method that was similar to that of CAI. Zong-tao *et al* (1985) but different in that it was done in a UHV system, and was monitored by a quadrupole mass spectrometer, rather than by chromatography.

Some samples were heated to temperature T, 350 C.>T<600 C and measured using FTIR while others were heated to T > 600 C and measured. However due to problems with heating, and temperature measurement, for the crystalline silicon substrates, the results were inconclusive. The lack of a 650 cm^{-1} bending mode and the uncertainty in the 2000 cm^{-1} peak added to the problems by making the hydrogen content determinations unreliable. Significant changes in the spectrum itself however warrant further investigation. Despite technical problems, which can be easily overcome the studies were promising enough to warrant further investigation. Further experiments are planned to study both the amount of hydrogen and the type of bonding present at different temperatures in our APCVD a-Si:H samples.

8. FURTHER OPTICAL MEASUREMENT TECHNIQUES

The standard method used for optical measurement of film thicknesses for a-Si:H films with stainless steel substrates has been reported briefly in the previous progress report (Clare *et al* 1987). A more complete description of the technique can be found in Phillips (1986). Using this technique films can be measured with thicknesses in the range ~ 0.55 - > 6 μm. It has however proven inadequate for measuring films thinner than 0.55 μm. The nature of more recent experiments lead to a need to develop new methods to determine the thickness of these thinner films. Surfometer techniques have proven unsuitable for measurements on stainless steel substrates because of their uneven surface. Two suitable methods have been developed to measure films with thicknesses less than 0.55 μm. These are the observation of visible coloured fringes and the use of sodium light interferometry with monochromatic (Sodium) light. These two methods are described below.

8.1 Measurement of Film Thickness Using Visible Coloured Fringes

During the early stages of a normal deposition several sets of coloured fringes are clearly visible on the surface of the samples. They consist of three to four clearly distinguishable, repeated, cycles of red, blue and then silver fringes. These eventually blend to give a uniform metallic surface and finally the normal specular colour distinctive of our APCVD samples. These fringes are thickness dependent and are due to destructive interference in the blue and red regions of the visible spectrum within the film itself. Consequently they are an ideal method for easily determining the thickness of very thinly deposited films.

For white light (visible), 0.4 μm < λ_{in} > 0.7 μm, if the pathlength of light in the film ($2d_1n_1$) is equal to half an integral number of wavelengths of a given λ_{in} then destructive interference will occur (figure 1). As that wavelength is absent from the reflected light the appearance of the film will be due to the remaining wavelengths, hence, the first fringe expected, that due to destructive interference of short wavelengths (~ 0.45 → 0.49 μm, blue light) appears red. The film thickness is given by $2d_1n_1 = \frac{1}{2}\,0.474$ or $d = \frac{\lambda_{in}}{2\,2_{ni}}$.

For first red fringe given n ~ 3.5 and λ_{in} = ~ 4.74×10^{-7} m d_1 = 0.034 μm. When the first blue fringe appears, due to the destructive interference of red light (~ 7.01×10^{-7} μm), the thickness is 0.046 μm.

For the second cycle of fringes:-

$$\text{Red} \cdot 2d_1n_1 = \frac{3}{2} \times 0.474$$

$$d = 0.102\ \mu m.$$

Blue - d = 0.150 μm.

For the third set of fringes:-

Red - d = 0.169 μm.

Blue - d = 0.251 μm. *

For the fourth set of fringes:-

Red - d = 0.237 μm. *

Blue - d = 0.351 μm. *

For the fifth set of fringes:-

Red - d = 0.305 μm. *

Blue - d = 0.451 μm. *

* note: These coincide and lead to a metallic appearance resulting in no more clearly distinguishable sets of fringes being seen.

This technique, of observing visible coloured fringes, enables film thicknesses to be measured in the range ~ 0.034 → ~ 0.251 μm.

Figure 8.1 Optical arrangement for fringe measurement

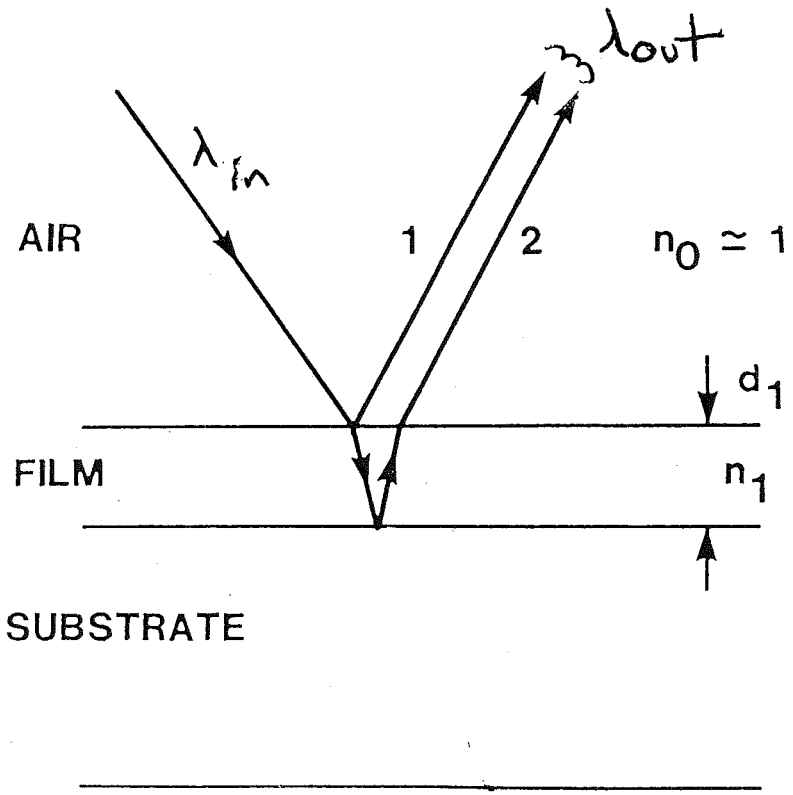

8.2 Measurement of Film Thicknesses Using Na Light Interferometry

To measure films with a thickness in the region between that covered by the coloured fringes and IR spectroscopy measurements the technique of Na light interferometry is used. Unlike the other methods described so far, this technique is destructive. The principal is similar to that used above except instead of white light a monochromatic sodium source is used.

For monochromatic light striking a thin film, eg, Sodium @ 0.559 μm a bright fringe will occur when a wavelength difference of $m\lambda_{in}$ occurs, where m = 0,1,2,3,4 ..... The film thickness is given by:

$$d = \frac{m\lambda_{in}}{2n}$$

$$= m \times 0.084\ \mu m$$

For our amorphous silicon films $n_1 = 3.5$ $d = m \times 0.084$ μm, hence leading to a series of fringes:-

0	1	2	3	4	5	6
d(μm) 0	0.084	0.168	0.252	0.337	0.421	0 .505

When a wavelength difference of $\frac{m\lambda_{in}}{2}$ occurs a dark fringe results and the film thickness is given by:

$$d = \frac{(2m+1)\lambda}{2\ 2_n}$$

Again our amorphous silicon films $d = (2m+1) \times 0.042$ m leading to a series of fringes:

0	1	2	3	4	5	6
d(μm) 0.042	0.126	0.210	0.294	0.379	0.463	0 .547

Before the thickness of a sample can be measured using interferometry part of the film must be etched off the stainless steel substrates to serve as a reference. To achieve this, part of the sample is dipped in a saturated solution of NaOH at ~ 70 → 80°C using a pair of tweezers until the a-Si:H is removed from the

Figure 8.2 Schematic diagram of N_a Interferometer system.

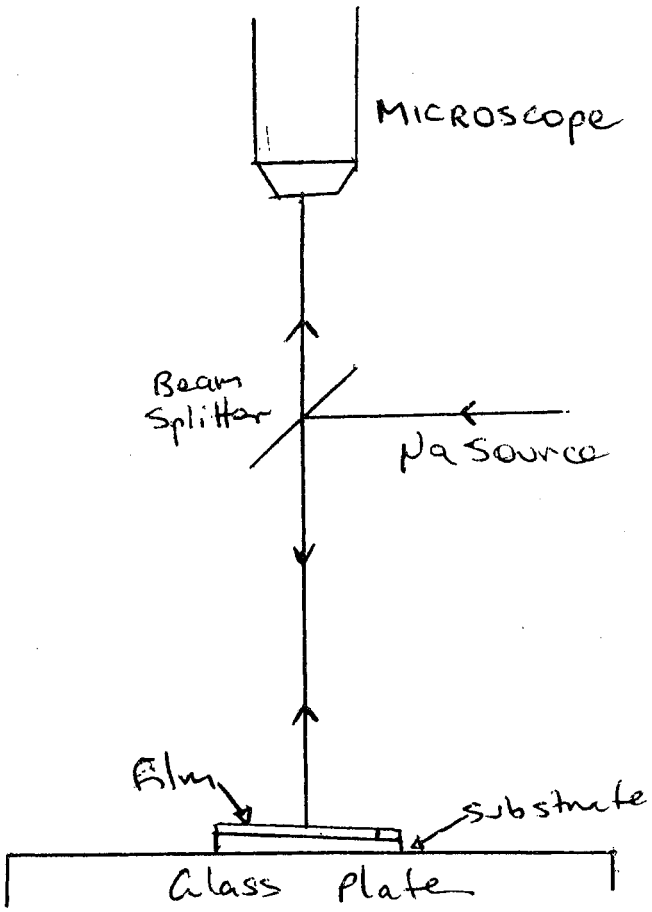

submerged section. The sample is then rinsed in distilled water, blown dry using N_2 or air and placed in the interferometer system. A schematic diagram of the interferometer system is shown in figure 8.2.

The experimental equipment itself is shown in figure 8.3.

The lens and glass plate held by the clamping rings were placed upon the travelling microscope stage and adjusted until the fringes were visible. The eyepiece was focussed by moving it up and down and the light source adjusted to give a maximum amount of light and good contrast in the fringes. Having centered the microscope over the interface between bare metal and film the number of dark or light fringes are counted. Film thickness can be calculated as above.

Using the current method of etching it is usually only possible to measure films with up to six distinguishable dark fringes. Attempts to induce partial etching on samples thicker than this have been unsuccessful. Therefore this leads to a measureable thickness range for this method of ~ 0.042 → 0.547 μm.

Attempts are currently being made to apply ellipsometry to the measurement of film thicknesses. This method coupled with one or more of the current methods will result in increased accuracy and precision in the thicknesses measured.

Figure 8.3 Interferometer experimental arrangement using Sodium Light.

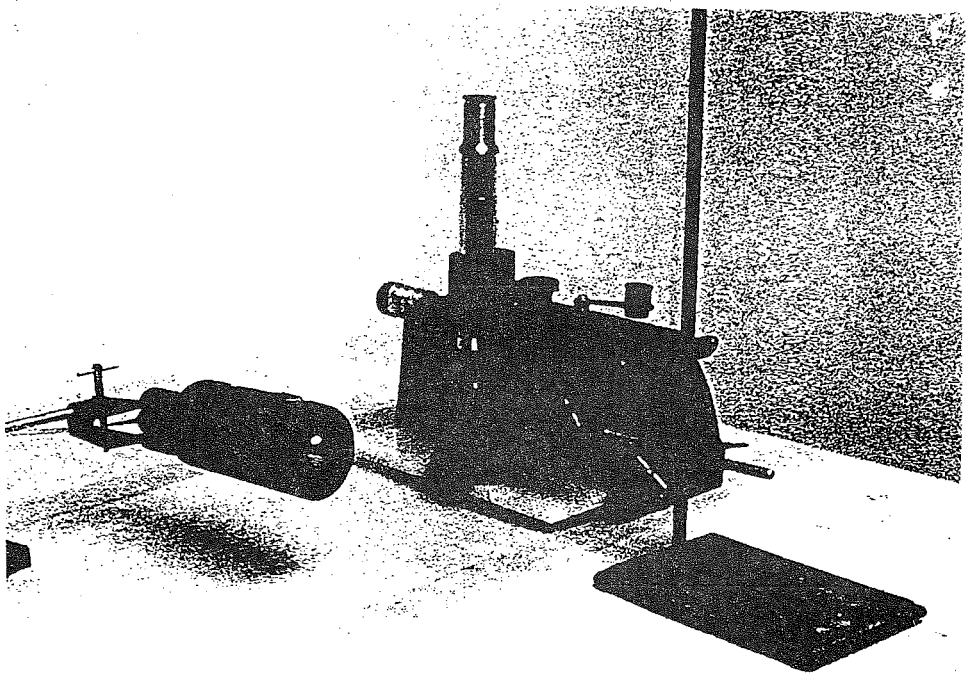

9. CHARACTERISATION OF A-Si:H FILMS USING S E M

The previous progress report (Clare *et al* 1987) has noted that one form the deposition may take has an opalescent appearance. Such an opalescent region is sometimes seen on the surface of our normally specular APCVD a-Si:H cells. This is particularly true of those cells with thicknesses of 3μm or greater. The cause of the opalescence is uncertain and it seems to be indiscriminantly distributed in respect to which runs and in which position on the block it occurs. SEM has been used to investigate this problem and the results are presented as well as suggestions as to the origin of the opalescence.

SEM has also been used to investigate the prevalence of shorting problems with prepared Schottky cells having thicknesses in the range 0.5 to 1.0 μm. The results show that the application of the silver contact spots is one of the major contributions to the shorting problems and that with some technical changes the shorting can be considerably reduced.

9.7 Opalescence on Samples with Stainless Steel Substrates

Initial studies using SEM investigated samples deposited on stainless steel substrates with varying degrees of opalescence on the surface. These samples are shown in table 9.1.

It can be seen in figures 9.1 and 9.2 that the difference between a normal and an opalescent surface appears to be the increased density of spherical globules visible on the surface of the opalescent sample (figure 9.2). This is further reflected in figure 9.3.

The difference as visible on the one sample is shown in figures 9.4 and 9.5. Figure 9.4 was taken over an opalescent area whereas figure 9.5 was taken over a specular area on the same surface.

Figure 9.6 taken on the most opalescent sample shows severe globule coverage.

TABLE 9.1

Sample	Thickness	Description
445	3.4	Normal specular sample, no opalescence present on the surface used as a standard.
448	4.9	Slight opalescence covering the whole surface. Essentially retains its shiny specular appearance.
456	3.7	Opalescence covering about three quarters of the surface. Remainder of sample retains specular appearance.
510 & 502	1.1 & 008	Surface entirely covered with a dull grey opalescence and random speckles scattered across the face.

FIGURE 9.1

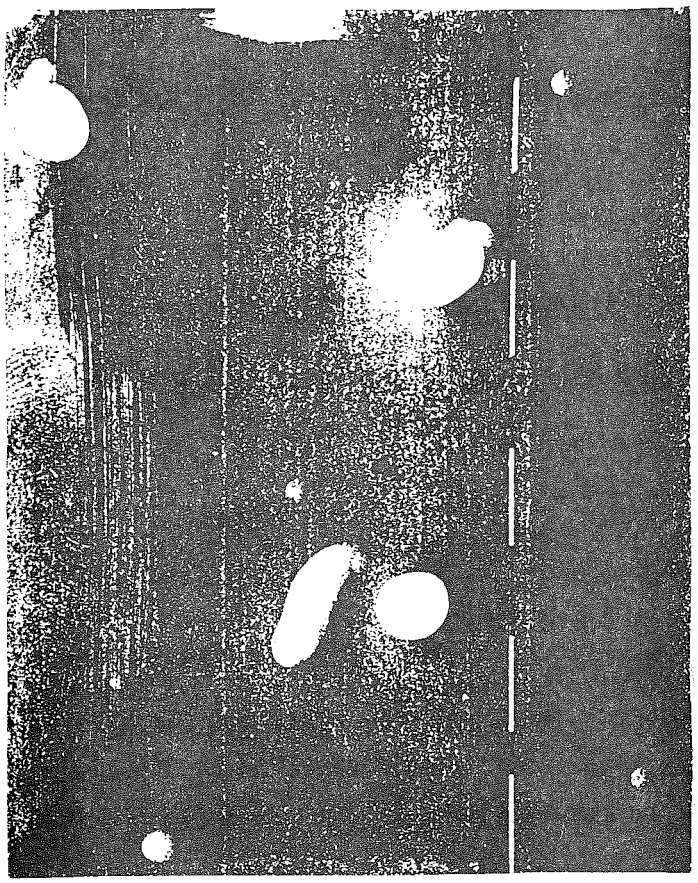

FIGURE 9.2

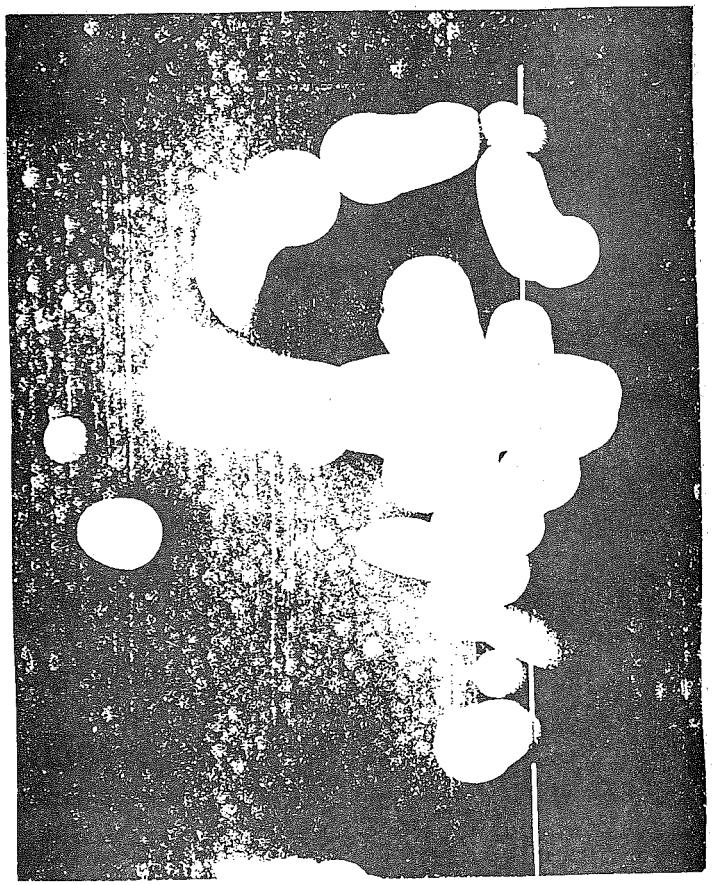

FIGURE 9.3 SEM photograph of sample surface

FIGURE 9.4 SEM Photograph of sample surface

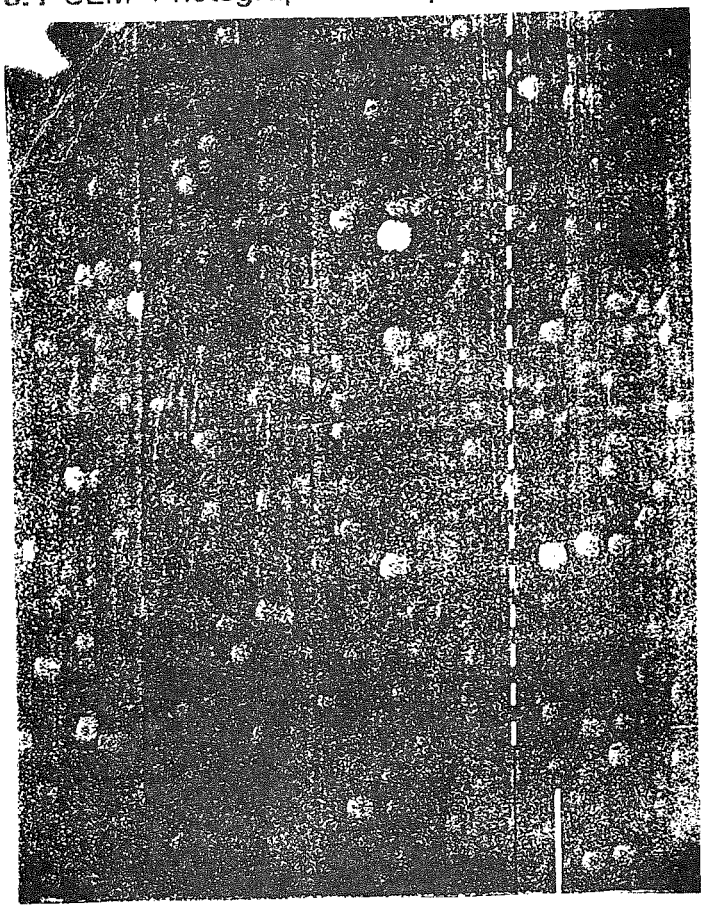

FIGURE 9.5 SEM photograph of sample surface

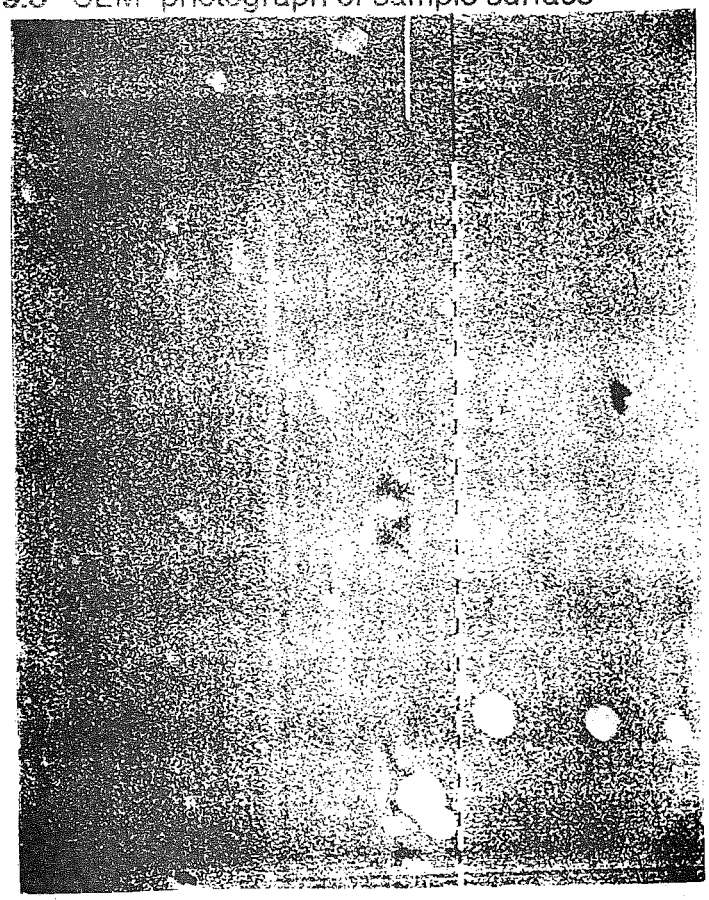

FIGURE 9.6 SEM photograph of sample surface

9.2 Opalescence on Samples with Crystalline Silicon Substrates

The same problems with opalescence is found on samples with crystalline silicon substrates as those found with samples on stainless steel substrates. Those samples which undergo several depositions appear to be the worst affected. All of these multiple depositions appear to be the worst affected. All of these multiple depositions, so far, are a dull dark grey colour with shiny speckles scattered across the surface, whereas the single depositions are a light grey colour, or even specular. Again a standard, specular sample was compared with opalescent samples using SEM. These samples are shown in table 9.2.

The same phenomena noted on the stainless steel samples is even more visible on the crystalline silicon samples. The difference between the specular surfaces and the opalescent surfaces are quite marked, as shown in figures 9.7 and 9.8. Clearly visible in figure 9.9 is one of is one of the shiny speckles found on the opalescent samples. These appear to be areas of the crystalline silicon substrate where the overlying a-Si:H layer has flaked off. This is demonstrated clearly in figures 9.10 and 9.11 where the region has been photographed at higher magnification. The opalescent area is shown (figure 9.11) and can be compared with the normal specular surface within the shiny region (figure 9.10).

Flaking of the overlying film is not unexpected considering their thickness. Flakes are also visible in the plastic bags used to store the samples. This flaking is not experienced with the thinner single deposition films on crystalline silicon.

TABLE 9.2

Sample	Thickness µm	Description
S106	~3	Specular surface, deposited in single deposition. Used as a standard.
S114	~9	Dull grey colour with speckles covering the surface. Deposited over 3 depositions, left under hydrogen between each one.
S104	~12	Deposited over 4 depositions in the same manner as S114. A dull (darker) grey colour with speckles most affected sample

FIGURE 9. 7 SEM photograph of sample surface

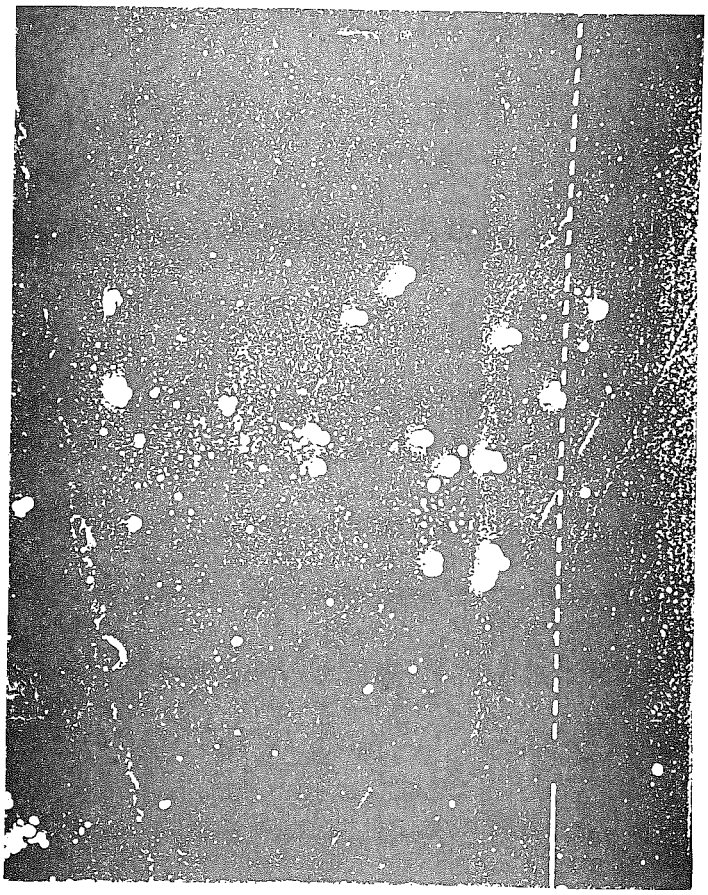

FIGURE 9.8 SEM photograph of sample surface

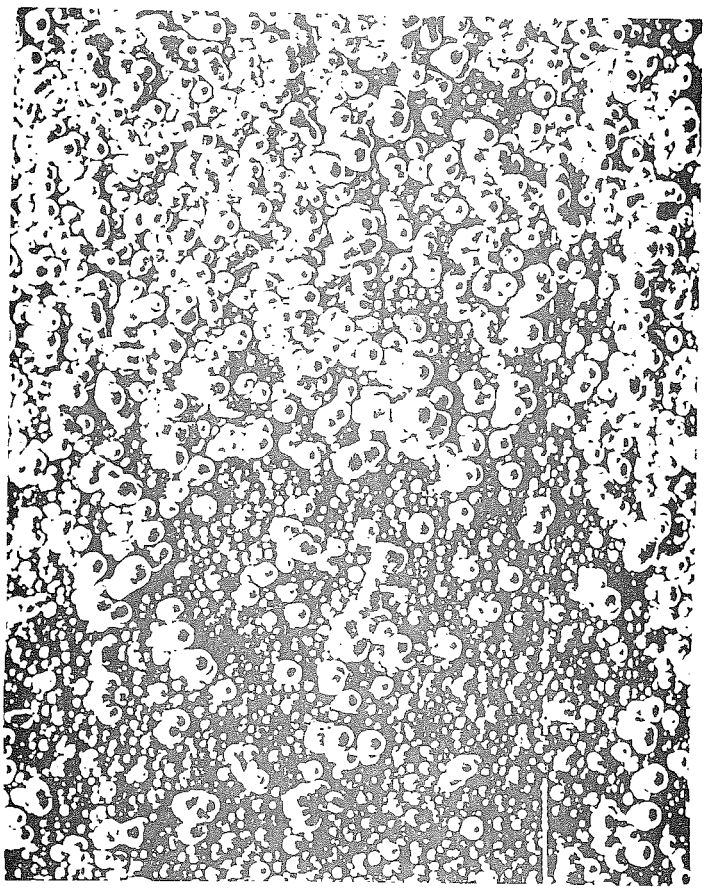

FIGURE 9.9 SEM photograph of sample surface

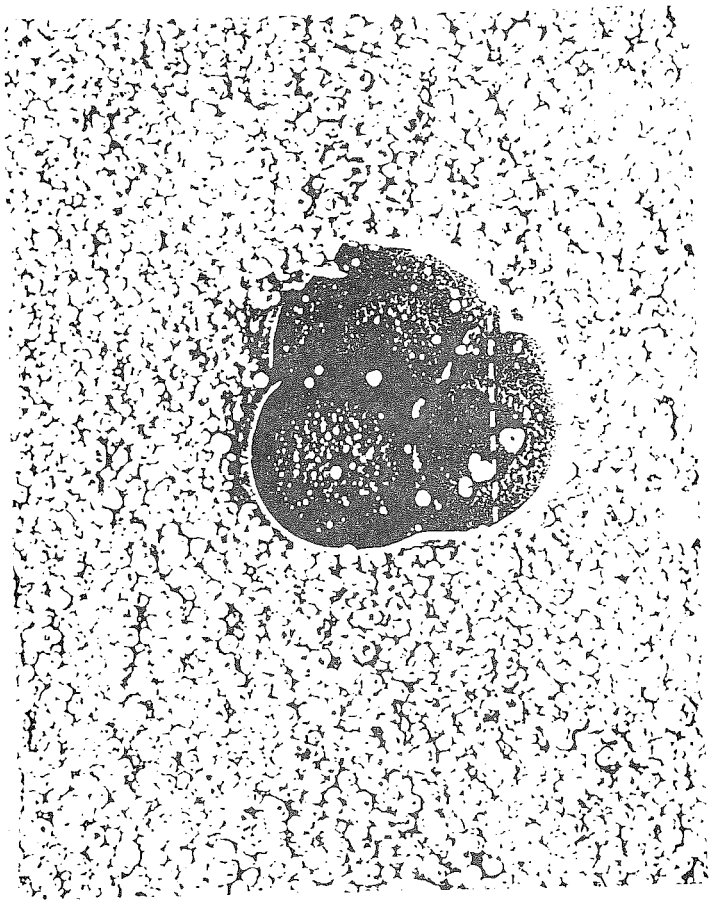

FIGURE 9.10 SEM photograph of sample surface

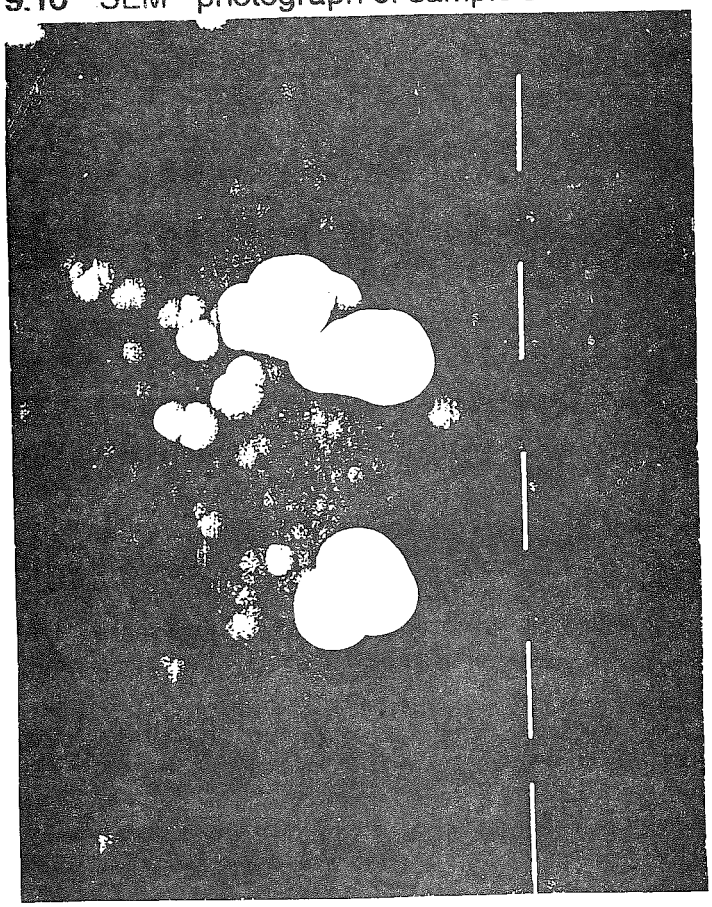

FIGURE 9.11 SEM photograph of sample surface

FIGURE 12 SEM Photograph of sample surface

9.3 Composition and Possible Causes of Opalescence

The composition and causes of the dense conglomeration of globules that results in the opalescence is not yet very well understood. It is known that for samples on crystalline silicon substrates, at least, multiple depositions on the same sample cause opalescence on all the samples in the same run. With thicker (> 0.5 μm) films on stainless steel substrates however it appears to be indiscriminant in respect to not only which runs it occurs in but to which position on the block within a single run.

It has been noted that the problem seems to be, to a certain degree, thickness dependent. Depositions of 3 μm or more seem to be more susceptible than thinner runs. Opalescent films are seen rarely for samples of 0.5 to 1 μm and have not yet been seen at all for samples of a few coloured fringes.

Figure 9.12 shows the surface of a film typical of those a few coloured fringes thick. It was deposited during the same period as the opalescent films on stainless steel mentioned previously. As can be seen, although the sample surface is pitted with craters no globules are yet visible. This seems to rule out such things as atmospheric dust acting as nucleating particles as these would be visible on the surface even at this stage in the deposition. The absence of any sign of globules at this stage in the deposition tends to suggest that they form at a later stage in the deposition and come from within the deposition system itself.

Compositional investigation using EDAX has shown that the cloudy globular region (and even single globules themselves) have the same composition as the normal surface. EDAX analysis however only confirms that the globules are silicon based and are not due to gross contaminants such as organics or other contaminants introduced by handling or the substrate preparation technique. Furthermore it is only a surface analysis technique and cannot tell the oxidation state of the silicon in the globule. Initial XPS depth profile studies performed during other experiments seem to suggest that the opalescent areas contain much larger atom percentages of oxygen than normal specular areas. As oxygen contamination is one possible cause of the opalescence further investigation needs to be performed in UHV using XPS or Auger.

Such studies involving shattering or depth profiling and Auger or XPS analysis are planned to further determine the nature and constituency of the globules.

Two other suggestions, apart from oxygen contamination, for the possible causes of the opalescence are:

1. water vapour not removed by the molecular sieves;

or 2. dust from the deposit that forms in the cooler parts of the APCVD deposition tube.

The true reason for the seemingly indiscriminant occurrence of the cloudiness between different runs and within the same run is still uncertain, as is the true nature of the globules causing it. Further investigation will be needed to ascertain the most likely cause of the opalescence so that it can be avoided in future depositions.

9.4 Silver Spots and Schottky Cell Shorting Problems

In an effort to explain why reducing the a-Si:H deposition to the optical optimum of ~0.7 μm greatly increased the incidence of shorting in completed Schottky cells an SEM investigation was done. It showed that one possible cause of the increase lay in the technuique used to apply the collector spots. Spots are sputtered onto the surface of the deposited film in the configuration shown in figure 9.13.

An SEM photograph taken of one spot on a sample with shorting showed (figure 9.14) that some of the Ag spots were displaced and made direct contact with the silicon. Because silver is known from previous experiments (Clare *et al* 1987) to be very mobile in silicon it is thought that the Ag from the spot may have migrated to the back contact, causing the spot to short.

To further confirm this a completed Schottky cell (n/o 546) was photographed using SEM over the whole surface and this was then compared with the electrical results for the same spots. The electrical map showing the open circuit voltage (Voc) for each spot, and the corresponding SEM photo, showing the physical nature of each spot, is shown in figures 9.15 and 9.16.

As can be seen from these two figures there seems to be a good correlation between those spots that give short circuit currents and those with a displaced silver spot. This further confirms that one main reason for the shorting on the thin film (0.5 to 0.7 μm) Schottky cells measured is due to this technical problem.

FIGURE 9.13 Arrangement of films in Schottky diode device.

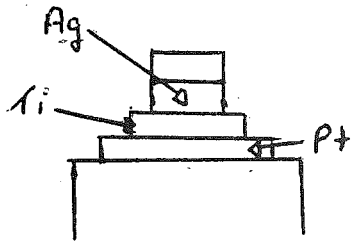

FIGURE 9.14 SEM photograph showing lack of registry of Silver and platinum spots.

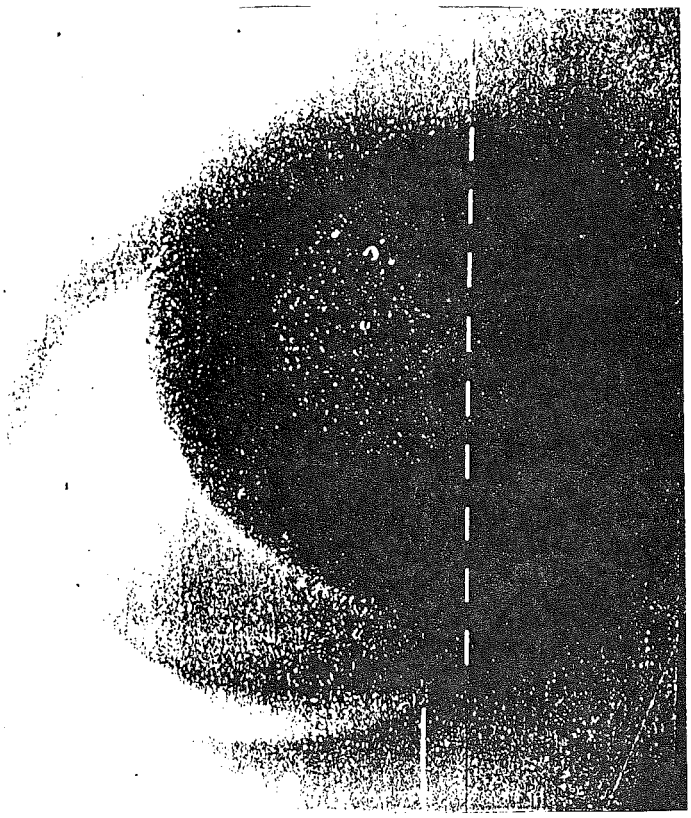

FIGURE 9.15 Arrangement of films in Schottky diode device.

Preanneal 250°C/20mins
Pt 7·2A/50sec
Ag 4A/30sec

350	0	0	0	0	0
270	335	190	0	0	387
1	342	0	0	0	0

Imax = 2·5μA.

FIGURE 9.16 SEM photograph showing lack of registry of Silver and platinum spots.

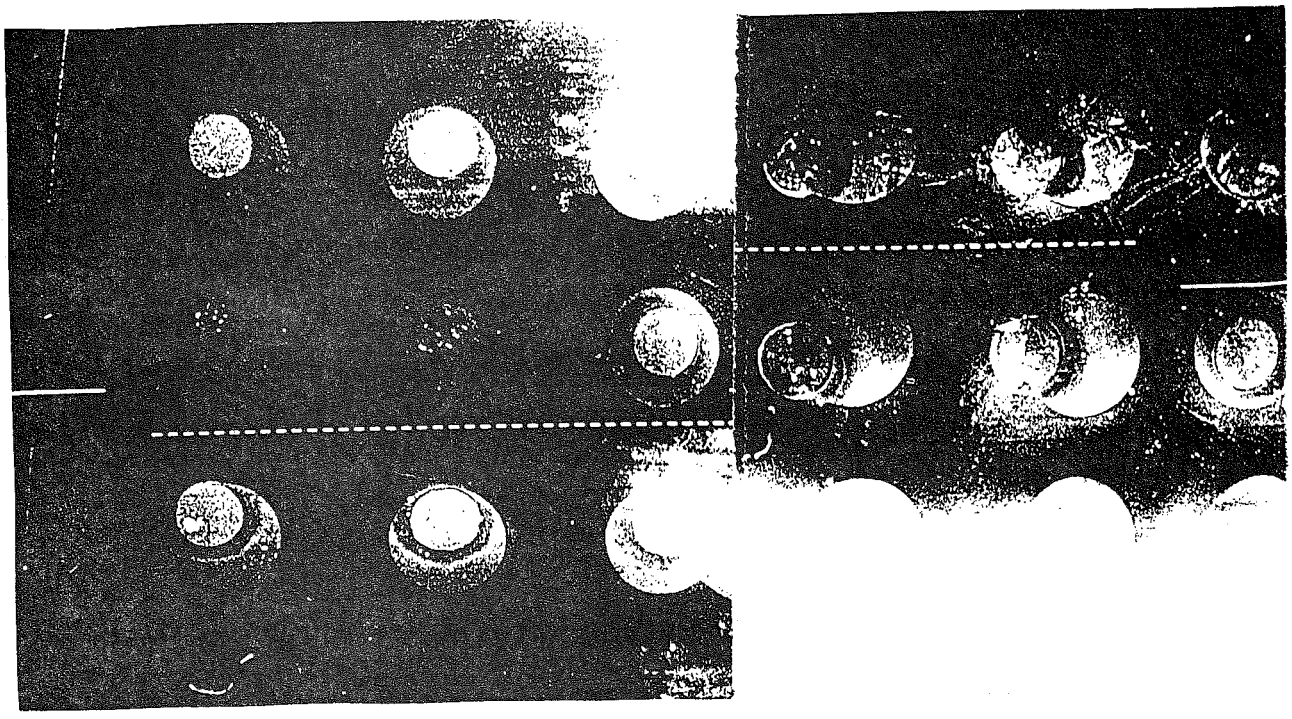

To overcome this problem subsequent cells were measured using only the platinum backing spot. Tests done by (Cheah 1987) on his RF sputtered samples showed no significant difference between electrical measurements taken with the Ag spot and those with only the platinum spot. Results for our APCVD cells, using the new technique, showed a greatly increased number of cells without the shorting problems and therefore more truly reflective of the nature of the underlying silicon surface. Figure 9.17 shows a cell (N/o 610) deposited under similar conditions to 564 but with only the Pt spots as collectors. Subsequent, more extensive, use of this technique has shown it to work quite satisfactorily.

This alteration to the technique for measuring the electrical characteristics has not entirely removed the problem of shorting for all cells, as surface faults still occur, but has removed the problems due to silver spot migration and has significantly reduced the incidence of shorting. It would appear that if the Ag spot method is to be used care must be taken in applying the spots, to ensure they do not overflow the platinum backing spots. If this does occur the silver may diffuse through a thin a-Si:H film and cause shorting with the back contact. If spot measurements are being used it is suggested that only the platinum spots be used as the front contacts as this not only avoids the shorting problem but also enables a faster turnover of samples. Only if full cells are being measured should there be a need to use a full configuration as shown in figure 9.13 and care must be taken when doing so.

FIGURE 17 Performance data for Schottky devices using only Platinum spots.

260	303	307	315	326	335
220	221	300	329	314	341
300	303	300	300	322	345

10. ELECTRON DIFFRACTION

For this investigation, thin amorphous Si films were deposited under our normal conditions on a KCl crystal. The crystal was dissolved and the a-si films were mounted on a set of Cu grids to be viewed through the Transmittance Electron Microscope and to allow electron diffraction on them. A. Philips 301 Electron Microscope was used for this purpose. The Electron diffraction pattern of the a-Si film (figure 9). The rings were diffuse suggesting short range order in the film. The radius of the ring R, d spacing (Distance between 2 adjacent planes on which the diffraction occurred) de Broglie wavelength of the electron λ and the distance between the specimen and the photographic plate L are related by

$$Rd = \lambda L$$

where λL is a constant for a particular Transmission Electron Microscope. In our case $\lambda L = 3.91 \times 10^{-12}\ m^2$.

a-Si is cubic. Hence from the first ring measurement the lattice spacing 'a' was calculated to be ~ 5.5 A°. (Table 10.1). These calculations were done for the electron diffraction pattern at different areas of the same film and the value of 'a' found to be similar. The first ring measurement suggests the plane of diffraction is (111)

The d spacings were calculated for the second ring and from that the Miller indices (hkl) for the corresponding planes were found (Table 10.2). Because the second ring was diffuse the inner and outer radius of the ring were taken and the d spacing were calculated for each radius. The plane corresponding to the inner radius (220) and that corresponding to the outer radius (311). These planes are that of Si.

The diffuse second ring suggests that the Si film has short range order.

The lattice spacing of the a-Si film is ~ 5.5Å.....Taking into consideration that the crystalline Si is tetrahedrally bonded with one atom at (0, 0, 0) and other at $\left(\frac{1}{4}, \frac{1}{4}, \frac{1}{4}\right)$. The shortest bond length 'ℓ' will be given by

$$\ell = \frac{\sqrt{3}}{4}\ a.$$

$$= 2.4Å$$

Similar measurements were done on a-Si films deposited under higher Hydrogen pressure (Figure10.2) presuming that the film has high Hydrogen concentration. These films gave similar electron diffraction pattern and the calculations for bond length gave the same values.

FIGURE 10.1 TEM electron diffraction image for thin a-Si film.

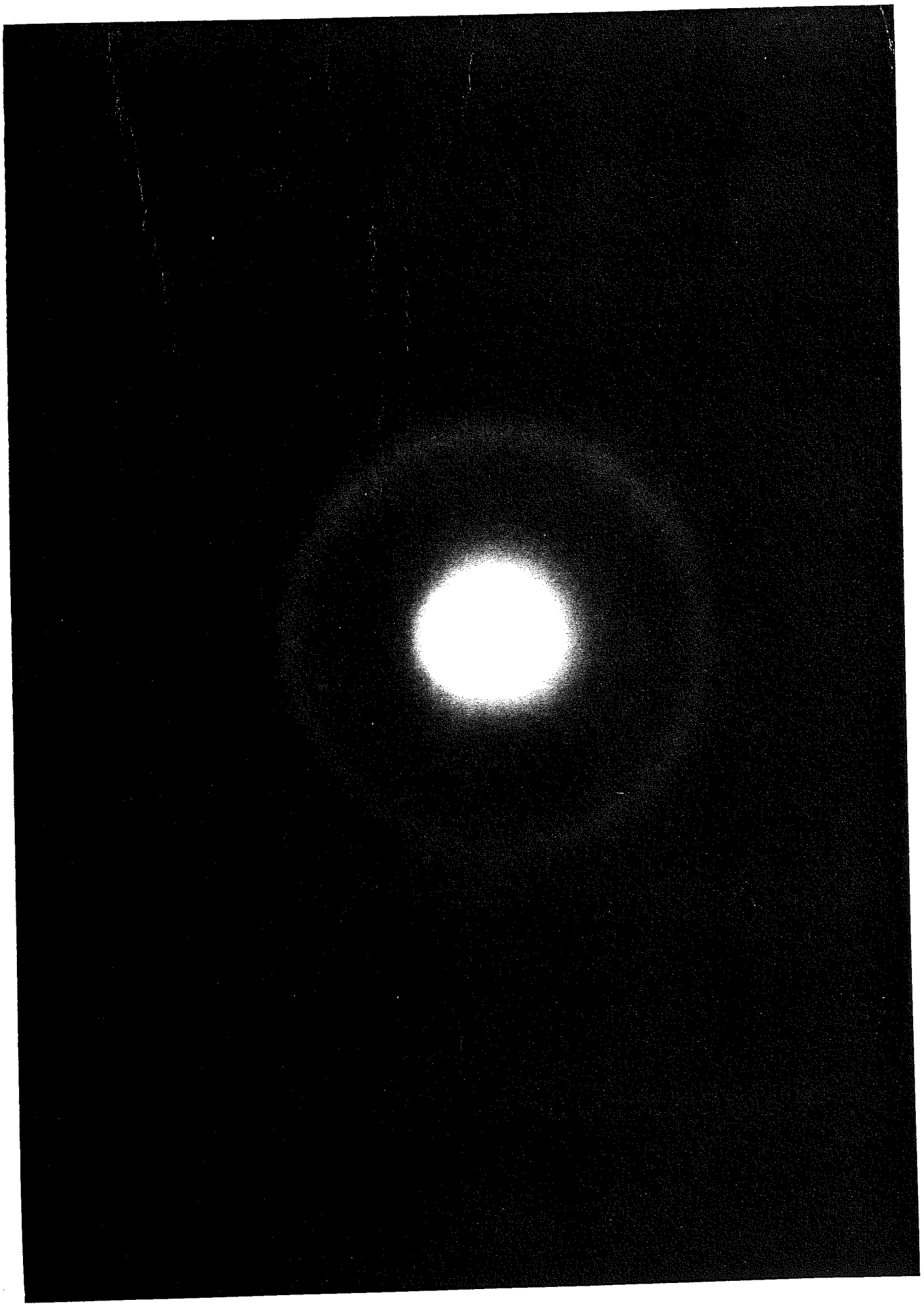

FIGURE 10.2 TEM electron diffraction image for thin a-Si film.

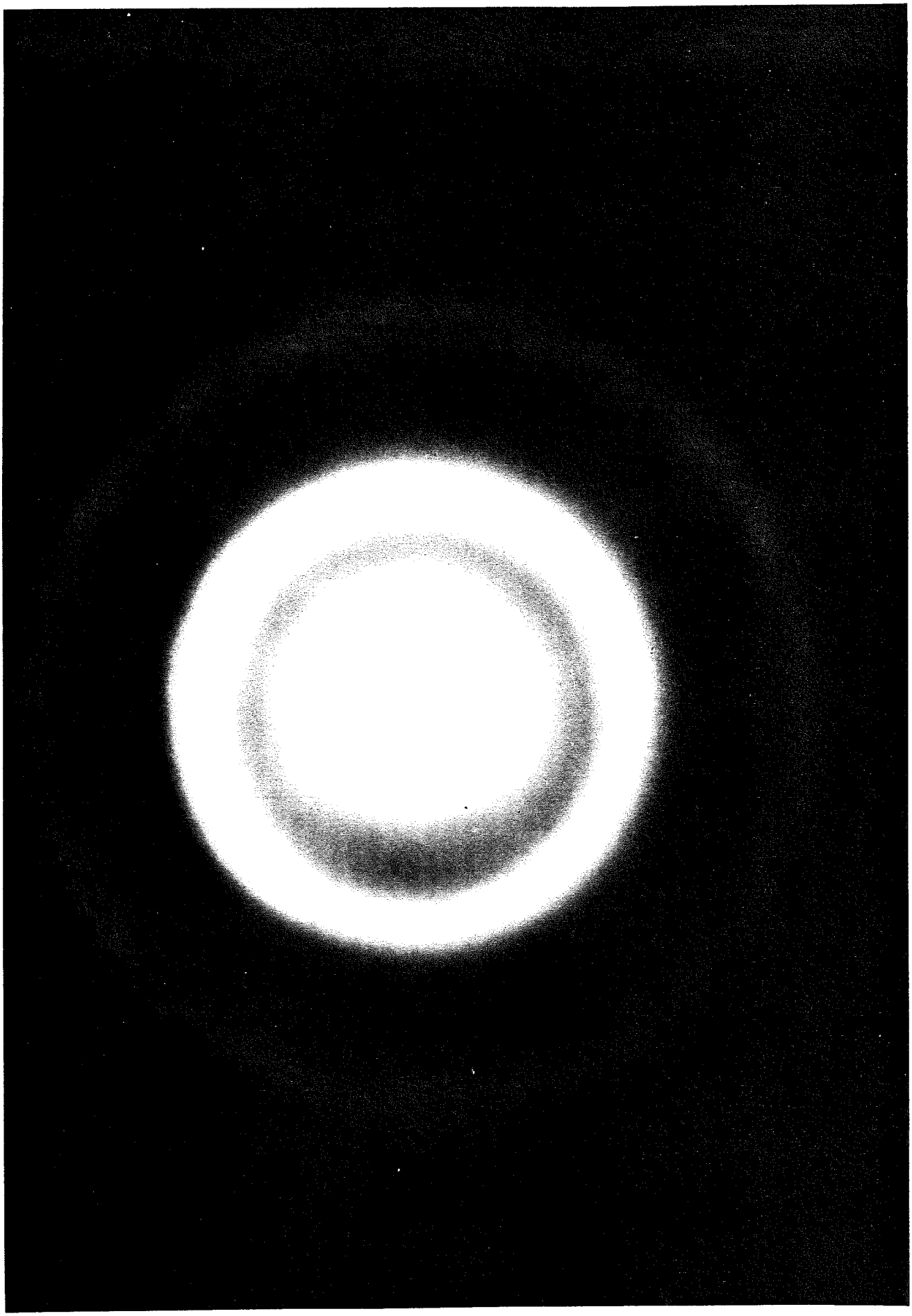

TABLE 10.1

RING 1 (first ring)

Plate No.	Radius (cm)	d spacing Å	Plane	Calculated a Å
2018	1.235	3.2	(111)	5.54
2019	1.270	3.1	(111)	5.37
21020	1.286	3.04	(111)	5.27

TABLE 10.2

Ring 2 (second ring)

Plate No.	Radius (cm)	d spacing Å	$h^2+k^2+\ell^2$	Plane
21018	*Rinner = 2.000	1.955	8.038 ≈ 8	(220)
	*Router = 2.355	1.660	11.14 ≈ 11	(311)
21019	*Rinner = 2.115	1.85	8.43 ≈ 8	(220)
	*Router = 2.44	1.6	11.26 ≈ 11	(311)
21020	*Rinner = 2.125	1.840	8.19 ≈ 8	(220)
	*Router = 2.45	1.596	10.89 ≈ 11	(311)

11. CONCLUSION

The work described in this report includes a number of investigations of methods to improve the quality and deposition rate of hydrogenated amorphous silicon films based on the atmospheric pressure chemical vapour deposition process using mixed silanes generated in situ from Mg_2Si. We also have described the results of a variety of characterisation techniques.

The APCVD process we have used is clearly limited in that although we can consistently deposit stable uniform films, their photovoltaic performance is poor. Major reasons for this include:

low hydrogen content as a result of the high deposition temperature

high series resistance due to oxide layers at the substrate interface and the top contact

The process however has considerable promise and we plan to investigate modifications to both the deposition technique and the device fabrication process to reduce the problems encountered.

We now have a reliable set of techniques for characterising the material and devices produced that will enable us to evaluate rapidly and comprehensively thin films of amorphous materials produced by future methods.

12 ACKNOWLEDGEMENTS

We wish to acknowledge the financial assistance under the SERIWA Grant 526/233/1 and the supplementary grant provided by the Hon. David Parker Minister for Minerals and Energy following the dissolution of SERIWA.

12 REFERENCES

Akhtar, "Preparation of ultra-high purity higher silanes and germanes", Synth. React. Inorg. Met-org. Chem., **16** (5) 729-748 (1986)

Austin E R and F W Lampe, J. Phys. Chem., 80 2811 (1976)

Bhattacharya, Guha S, Krishna K V and Bapat, J. Appl. Phys. **53** (9) 6285 (1982).

Burnham N A, Schwartzlander A B, Nelson A J and Kazmerski L L Solar Cells **21** 135-140 (1987).

Biegelsen D H , Street R A, Tsai C C and Knights J C, Phys. Rev. **B 20** (12) 4839 (1979).

Cai Zong-tao, Ke-lun HE, Li Zi-an and Cheng Ru-guang Solar Energy Mater. 12 43-50 (1985).

Cheah Swee Hoc "Amorphous Silicon Devices" M. Eng. Sci. Thesis (1987).

Chek K P, Yu C K, Lim P K John P K and Wong S K, Physical Review **B 30** (6) 34422 (1984).

Christ H J, Schwanke D, Th Uihlein and Sockel H G J. Phys. E: Sci. Instrum. **19**, 793-798 (1986).

Clare B W, Cornish J C L, Hefter G T, Jennings P J, Lund C P, Phillips S R, Raikar G N Thambirasa G P, Cheah S H, Livingstone J, Klauber C, "Amorphous Silicon Solar Cells", Research Report, Murdoch University (1987).

Corderman R R and Vanier P E, J. Appl. Phys. **54** 3987-3992 (1983).

Den Boer W, J. Phys. (Paris) **42** C4-451 (1981).

Ellis D B Jr and Gordon R G, J. Appl. Phys. 54 5381 (1983)

Freeman E C and Paul W, Phys.Rev. b**18** (8) 4288 (1978).

Fritzche H, Taielian M, Tsai C C and Gazei P J, J. Appl. Phys. **50** 3366-3370 (1979).

Fritzche H, Solar Cells **2**, 289 (1980).

Gangopadhyay S, Iselborna S, Rulech H , Scroder N amd Geiger G. Philos. Mag. **B 51** (3) L33-L38 (1985)

Gangopadhyay S, Schroder B and Gieger J, Philos. Mag. **B 56** (3) 321 (1987).

Gokhale S D, Drake J E and Jolly W L, J. Inorg. Nuc. Chem. **27** 1911-1916 (1965).

Gunzel E, Proceedings of ISPC-7, 171-176 (1985).

Hegedus Steven R, Rocheleau R E, Cebulka J M and Baron B N, J. Appl. Phys. **60** 1046-1054 (1986).

Hiden Analytical, Library list of Cracking Patterns (1985).

Kurtz S R, Prozcia J and Gordon R G, J. Appl. Phys. **54** 5381-53 -- (1983)

Kurtz S R, Prozcia J and Gordon R G, J. Appl. Phys. **59** 249-256 (1986).

Longeway P A, Weakliem and Estes R D, J. Appl. Phys. **57** 5499-5505 (1984).

---------- J. Phys. Chem **88** 3282-3287 (1984).

----------, J. Phys. Chem. **88**, 73-77 (1984)

Lukovsky G in "Fundamental Physics of Amorphous Semiconductors" ed. Yonezawa F Springer Verlag (1981).

Lund CP, Honours Thesis Murdoch University (1987).

Mackenzie, LeComber P G and Spear W E, Philos. Mag. **B 46**, 377 (1982).

McMillan A and Peterson E M, J. Appl. Phys. **50** 5238-5240 (1979).

Madden H H and Hjalmarson H P, J. Vac. Sci. Technol. **20** 502-505 (1982).

Madden H H, J. Vac. Sci. Technol. A 1 1201-1204 (1983).

Matsumura H, Jpn. J. Appl. Phys **25** L949-L951 (1987).

Matsumura H and Tachibana H Appl. Phys. Lett. **47** 833 (1985).

Maycock P Photovoltaics International, January 5 (1986).

Meaudre M and Meaudre R, Phil. Mag. **B 55** 417-426 (1987).

Morimoto A Kobayashi I, Kumeda M and Shemizu, Jpn. J. App. Phys. **25** L752-L754 (1986).

Mutsukura N, Katoh Y and Machi Y, J. Appl. Phys. **60** 3364 (1986).

Oda S, Ishihara S, Shibata N, Shirai H, Miyauchi A, Fukuda K, Tanabe A, Ohitoshi H, Hanna J and Shimizu I, Jpn. J. Appl Phys. **25** L188-L190 (1986).

Orton J W and Powel M J, Philos. Mag. **B 50** 11 (1984).

Phillips S R, Honours Thesis, Murdoch University (1986).

Powell M J and Pritchard J, J. Appl. Phys. **54** 3244 (1983).

Robertson R and Gallagher A, J. Appl. Phys. cb593402-3411 (1986).

Saraie J, Fujnh Y, Yoshimoto M, Yamazoe K and Matsunami H, Thin Solid Films **117** 59 (1984).

Schwartzlander A B, Asher S E, and Kazmerski L L, J. Vac. Sci. Technol. A4 1570-1573 (1986).

Shanks H, Fang C.J. Ley L, Cardona M, Desmond F J, and Kalibitzer, Phys. Stat. Sol. **6 100** 43 (1980).

Shibata N, Fukuda K, Ohtoshi H, Hanna J, Oda and Shimizu I, Jpn. J. Appl. Phys **26** L10-13 (1987).

Smith R J and Strongin M, Phys. Rev. **B 24** (10) 5863 (1981).

Smith Z E, Chu V, Shepard K, Aljishi S, Slobodin D, Kolodzey J, Wagner S, and Chu T L, Appl. Phys. Lett. **50** 1521-1523 (1987).

Spanier E J and MacDiarmid A G, Inorganic Chemistry 1, 432-433 (1962).

Spear W E and Le Comber P G, Non-cryst. Solids 9-10 7827 (1972).

Soloman I, Benferhat and Tran Quoc H, Phys. Rev. **B 30** 3422-3129 (1984).

Stoddart C T H and Hondros E D, Nature (Phys. Sci.) **237** 90 (1972).
Weisfield R L, J. Appl. Phys. **54** (11) 6401 (1983).

Yarwood J, "High Vacuum Technique" 4th Edn. Chapman and Hall, London (1967).

Yahya E and Shanks H R, Solar Energy Materials **16** 189-198 (1987).

Zajac G and Bader S D, Phys. Rev. **B26** 5688-5693 (1982).